ANALYSIS OF HIGH-G CAMERA SUPPORT STRUCTURE FOR CRASH TEST SYSTEM

A THESIS SUBMITTED TO
THE GRADUATE SCHOOL OF NATURAL AND APPLIED SCIENCES
OF
MIDDLE EAST TECHNICAL UNIVERSITY

BY

MAHMUT GÖKHAN ERDOĞDU

IN PARTIAL FULFILLMENT OF THE REQUIREMENTS
FOR
THE DEGREE OF MASTER OF SCIENCE
IN
MECHANICAL ENGINEERING

DECEMBER 2009

Approval of the thesis:

STRUCTURAL ANALYSIS OF CAMERA HOLDER AND PALETTE DESIGN

submitted by **M. GÖKHAN ERDOĞDU** in partial fulfillment of the requirements for the degree of **Master of Science in Mechanical Engineering, Middle East Technical University** by,

Prof. Dr. Canan Özgen
Dean, Graduate School of **Natural and Applied Sciences** _____

Prof. Dr. Süha Oral
Head of the Department, **Mechanical Engineering** _____

Prof. Dr. Mustafa İlhan Gökler
Supervisor, **Mechanical Engineering Dept., METU** _____

Prof. Dr. Haluk Darendeliler
Co-Supervisor, **Mechanical Engineering Dept., METU** _____

Examining Committee Members:

Prof. Dr. Y. Samim Ünlüsoy
Mechanical Engineering Dept., METU _____

Prof. Dr. Mustafa İlhan Gökler
Mechanical Engineering Dept., METU _____

Prof. Dr. S. Kemal İder
Mechanical Engineering Dept., METU _____

Prof. Dr. Haluk Darendeliler
Mechanical Engineering Dept., METU _____

Dr. Mustafa Erdener
Ford Otosan _____

Date: December 18th, 2009

I hereby declare that all information in this document has been obtained and presented in accordance with academic rules and ethical conduct. I also declare that, as required by these rules and conduct, I have fully cited and referenced all material and results that are not original to this work.

Name, Last name: M. Gökhan ERDOĞDU

Signature:

ABSTRACT

ANALYSIS OF HIGH-G CAMERA SUPPORT STRUCTURE FOR CRASH TEST SYSTEM

Erdoğdu, Mahmut Gökhan

M.Sc., Department of Mechanical Engineering
Supervisor: Prof. Dr. Mustafa İlhan Gökler
Co Supervisor: Prof. Dr. Haluk Darendeliler

December 2009, 84 pages

Sled Crash Test System is one of the key elements in todays high safety vehicle designs. In the crash test systems, high speed imaging by high speed cameras is required. For the success of high speed imaging, high speed cameras should be well secured on the sled of the system which is being accelerated to high-g values to simulate vehicle crash. In this study, structural analysis of the high – g camera support structure for the sled crash test sytem which is available in METU-BİLTİR Center Vehicle Safety Unit is carried out. For the secure connection of the high speed cameras, three different configurations of the camera support structure with different camera positions are analyzed by transient dynamic analysis. The finite element simulations are carried out under the acceleration of 90 g which is the maximum applicable acceleration on the system. After verification of the configurations with the computer simulations, one of the configuration has been tested at the sled test facility of METU-BILTIR Center Vehicle Safety Unit.

Keywords: Crash Test, sled test system, high speed imaging, camera holder support structure, high-g acceleration

ÖZ

ÇARPIŞMA TEST SİSTEMİ İÇİN YÜKSEK İVMEYE DAYANIKLI KAMERA DESTEK YAPISININ ANALİZİ

Erdoğdu, Mahmut Gökhan

Yüksek Lisans, Makina Mühendisliği Bölümü
Tez Yöneticisi: Prof. Dr. Mustafa İlhan Gökler
Tez Yardımcı Yöneticisi: Prof. Dr. Haluk Darendeliler

Aralık 2009, 84 sayfa

Sled Çarpışma Test Sistemi, günümüz yüksek güvenlikli araçların tasarlanmasında anahtar bileşen olmaktadır. Çarpışma test sistemlerinde yüksek hızlı kameralarla yüksek hızlı görüntüleme gerekmektedir. Yüksek hızlı görüntülemenin başarılı bir şekilde gerçekleştirilebilmesi için de yüksek hızlı kameraların, araç çarpışmasını simüle etmek üzere yüksek – g ivmelenme verilecek slede, sağlam şekilde sabitlenebilmeleri gerekmektedir. Bu çalışmada, METU-BİLTİR Merkezi Araç Güvenlik Birimi'nde mevcut bulunan sled çarpışma test sistemi için kullanılan yüksek – g kamera destek yapısının yapısal analizi gerçekleştirilecektir. Yüksek hızlı kameraların sağlam bir şekilde bağlanabilmeleri için, kameranın farklı konumlandırma şekilleriyle üç farklı konfigürasyondaki kamera destek yapısı dinamik analiz edilecektir. Sonlu eleman simülasyonları sisteme uygulanabilir en yüksek ivme olan 90 g altında uygulanmıştır. Konfigürasyonların bilgisayar simülasyonlarıyla desteklenmesinden sonra, konfigürasyonlardan bir tanesi METU-BİLTİR Merkezi Araç Güvenlik Birimi'nde test edilecektir.

Anahtar Kelimeler: Çarpışma testi, sled test sistemi, yüksek hızlı görütüleme, kamera tutucu destek yapısı, yüksek-g ivme

To My Family and My Fiance,

ACKNOWLEDGEMENTS

I would like to express my deepest gratitude to my supervisor Prof. Dr. Mustafa İlhan Gökler and my cosupervisor Prof. Dr. Haluk Darendeliler for their guidance, advice, criticism, encouragement and insight throughout the study.

I would like to thank to METU-BILTIR Center Vehicle Safety Unit for the tests performed during the experimental study.

I also wish to thank to my senior colleagues Ulaş Göçmen for his valuable support and assistance.

Further, thanks go to Halit Şahin, Ali Demir, Hüseyin Ali Atmaca and Osman Mumcu, for their endless efforts and aids.

I am deeply indebt to my parents, Gülsevim and Enver Erdoğdu, my sister Ayça Erdoğdu, my brother Gürkan Erdoğdu and my fiance Bahar Çat for their encouragement and faith in me.

TABLE OF CONTENTS

ABSTRACT iv

ÖZ v

ACKNOWLEDGEMENTS vii

TABLE OF CONTENTS viii

LIST OF TABLES xii

LIST OF FIGURES xiii

LIST OF SYMBOLS xviii

CHAPTERS

1. INTRODUCTION 1

1.1 Importance of Crash Test Systems 1

1.2 Crash Test System at METU-BILTIR Center 3

1.3 High Speed Imaging 9

1.4 The Camera Support Structure at METU-BİLTİR Center Vehicle Safety Unit 11

1.5 Scope of the Thesis 12

2. INPUTS AND PARAMETERS OF THE COMPUTER SIMULATIONS FOR THE CAMERA SUPPORT STRUCTURE 14

2.1 Configurations of the Camera Support Structure 14

2.1.1 Sled 16

2.1.2 Camera Holder Arms 16

2.1.3 Camera Holder Support Arms 17
2.1.4 Camera Holder 18
2.1.5 Camera Holder Profile 19
2.2 Finite Element Method for Transient Dynamic Structural Analysis 21
2.2.1 Equation of Motion 22
2.2.2 Mass Matrix 23
2.2.3 Damping of the System 24
2.2.4 Direct Integration Method 24
2.3 Finite Element Model 27
2.4 Material Properties 29
2.5 Bolt Connections 29
2.6 Finite Element Analysis Parameters 30
2.6.1 Enforced Motion Load for the Analyses 30
2.6.2 Time Steps and Termination Time for the Analyses 32
2.6.3 Boundary Conditions 33
3. COMPUTER SIMULATIONS AND RESULTS 34
3.1 Results of Maximum Displacement Values of Camera Lens Center 36
3.2 Visualization of the Displacement of Camera Lens Position 41
3.2.1 Displaced Model Shape of Configuration 1 in Region 2 41
3.2.2 Displaced Model Shape of Configuration 2 in Region 1 43
3.2.3 Displaced Model Shape of Configuration 3 in Region 3 44
3.3 Graphical Representation for the Displacement Results of Camera Lens Position 46
3.3.1 Displacement Graph for Configuration 1 at Center of Region 2 46

3.3.2 Displacement Graph for Configuration 2 at the Right Side of Region 1 48
3.3.3 Displacement Graph for Configuration 3 at the Right Side of Region 3 52
3.4 Stress Analysis for Camera Support Structure 55
3.5 Stress Distribution When the Maximum Stress Occurs 56
3.5.1 Stress Distribution for Configuration 1 at the Middle of Region 2 56
3.5.2 Stress Distribution for Configuration 2 at Right Side of Region 1 56
3.5.3 Stress Distribution for Configuration 3 at Right Side of Region 3 56
4. ANALYSES FOR ALTERNATIVE CAMERA HOLDER PROFILE AND CAMERA HOLDER OF CAMERA SUPPORT STRUCTURE 58
4.1 Analyses Results for Short Camera Holder Profile 58
4.2 Analyses for Alternative Camera Holder Design 61
5. CRASH TESTS 63
5.1 Crash Tests with the Dummy Camera 63
5.1.1 Dummy Camera 63
5.1.2 Test System with the Dummy Camera 64
5.1.3 Off-Board Cameras Used During the Test 65
5.1.4 Pulse Generation for the Test 66
5.1.5 Test Results 66
5.2 Crash Test with High-g High Speed Imaging Camera 67
6. CONCLUSIONS AND DISCUSSIONS 68
6.1 General Conclusion 68
6.2 Future Works 69
REFERENCES 71

APPENDICES

A. TECHNICAL INFORMATION OF CAMERA SUPPORT STRUCTURE COMPONENTS AT METU-BİLTİR CENTER VEHICLE SAFETY UNIT 73

A.1 Technical Specifications of Camera Holder Support Arms 73

A.2 Technical Specifications of Camera Holder Arms 75

A.3 Technical Specifications of Camera Holder Profile 76

A.4 Technical Specifications of Camera Holder 77

B. TECHNICAL INFORMATION OF SLED CRASH TEST SYSTEM, HIGH SPEED CAMERA AND DATA ACQUISITION SYSTEM AT METU-BİLTİR CENTER VEHICLE SAFETY UNIT 81

B.1 Technical Specifications of IST Sled Crash Test System [19] 81

B.2 Technical Specifications of Weinberger Vision Visario G2 High Speed Camera [20] 82

B.3 Technical Specifications of Kayser Threde Minidau Advanced Data Acquisition System [21] 83

LIST OF TABLES

TABLES

Table 2.1 Material Properties of Aluminum 6063 – T6 29

Table 2.2 Torque Values for Bolts and Screws 30

Table 3.1 Total Displacement Values in mm 37

Table 3.2 Displacement Values in X Direction in mm 37

Table 3.3 Displacement Values in Y Direction in mm 38

Table 3.4 Displacement Values in Z Direction in mm 38

Table 3.5 Recommendations for Configuration Type and Position of the Camera Holder 40

Table 3.6 Maximum Von Mises Stress Values in MPa 55

Table 4.1 Displacement Values with Long and Short Profiles at the Camera Lens Position 59

Table 4.2 Displacement Values with Long and Short Profiles at the Camera Holder Base Center 59

Table 4.3 Displacement Values with the Alternative Camera Holder 62

Table 4.4 Displacement Values with the Original Camera Holder 62

LIST OF FIGURES

FIGURES

Figure 1.1 Crash Test System at METU-BILTIR Center 4

Figure 1.2 Hydraulic System Schematic of Catapult System 6

Figure 1.3 Test Dummies Family..... 7

Figure 1.4 Minidau Advanced with 32 Channels 7

Figure 1.5 Lighting System..... 8

Figure 1.6 Visario G2 High Speed Camera 10

Figure 1.7 Visario G2 High Speed Camera 10

Figure 1.8 Configuration 1 of Camera Support Structure..... 11

Figure 1.9 Configuration 2 of Camera Support Structure..... 12

Figure 1.10 Configuration 3 of Camera Support Structure..... 12

Figure 2.1 Configuration 1 of Camera Support Structure..... 15

Figure 2.2 Configuration 2 of Camera Support Structure..... 15

Figure 2.3 Configuration 3 of Camera Support Structure..... 16

Figure 2.4 Sled of the Crash Test System..... 16

Figure 2.5 Camera Holder Arm 17

Figure 2.6 Assembly of the Camera Holder Arms with the Sled..... 17

Figure 2.7 Camera Holder Support Arm..... 18

Figure 2.8 Assembly of the Camera Holder Support Arms to the Sled and the Camera Holder Arms 18

Figure 2.9 Camera Holder 18
Figure 2.10 Camera Holder Profile 19
Figure 2.11 Camera Holder Profile Cross Section 19
Figure 2.12 Assembly of the Camera Holder with the Camera Holder Profile 20
Figure 2.13 Assembly of the Camera Holder with the Camera Holder Profile 20
Figure 2.14 Assembled Camera Support Structure 21
Figure 2.15 10 – Node Tetrahedral Element 27
Figure 2.16 FEA Model for Configuration I 28
Figure 2.17 FEA Model for Configuration II 28
Figure 2.18 FEA Model for Configuration III 29
Figure 2.19 Typical Deceleration Curve 31
Figure 2.20 Simplified Acceleration Curve 31
Figure 2.21 Enforced Motion Graph 32
Figure 2.22 Enforced Motion Application Part 32
Figure 3.1 Regions for the Sled 34
Figure 3.2 Sub-Regions for the Sled 35
Figure 3.3 Right Position of the Camera Holder in Region-1 for Configuration 1 35
Figure 3.4 Lens Center Position of the Camera 36
Figure 3.5 Axes Definition of the Camera Support Structure System 37
Figure 3.6 Best Configuration and Position of the Camera Holder for Region 1 39
Figure 3.7 Best Configuration and Position of the Camera Holder for Region 2 39
Figure 3.8 Best Configuration and Position of the Camera Holder for Region 3 40
Figure 3.9 The Exaggerated Displaced Model of Configuration 1
in the Left Side of Region 2 41

Figure 3.10 The Exaggerated Displaced Model of Configuration 1
in the Middle of Region 2 42

Figure 3.11 The Exaggerated Displaced Model of Configuration 1
in the Right Side of Region 2 42

Figure 3.12 The Exaggerated Displaced Model of Configuration 2
in the Left Side of Region 1 43

Figure 3.13 The Exaggerated Displaced Model of Configuration 1
in the Middle of Region 2 43

Figure 3.14 The Exaggerated Displaced Model of Configuration 1
in the Right Side of Region 2 44

Figure 3.15 The Exaggerated Displaced Model of Configuration 344
in the Left Side of Region 3 44

Figure 3.16 The Exaggerated Displaced Model of Configuration 3
in the Middle of Region 3 45

Figure 3.17 The Exaggerated Displaced Model of Configuration 3
in the Right Side of Region 3 45

Figure 3.18 Graph of Total Displacement for Configuration 1
At the Center of Region 2 47

Figure 3.19 Graph of Displacement in X Direction for Configuration 1
At the Center of Region 2 47

Figure 3.20 Graph of Displacement in Y Direction for Configuration 1
At the Center of Region 2 48

Figure 3.21 Graph of Displacement in Z Direction for Configuration 1
At the Center of Region 2 49

Figure 3.22 Graph of Total Displacement for Configuration 2
At the Right Side of Region 1 49

Figure 3.23 Graph of Displacement in X Direction for Configuration 2 At the Right Side of Region 1 50
Figure 3.24 Graph of Displacement in Y Direction for Configuration 2 At the Right Side of Region 2 51
Figure 3.25 Graph of Displacement in Z Direction for Configuration 2 At the Right Side of Region 1 51
Figure 3.26 Graph of Total Displacement for Configuration 3 At the Right Side of Region 3 52
Figure 3.27 Graph of Displacement in X Direction for Configuration 3 At the Right Side of Region 3 53
Figure 3.28 Graph of Displacement in Y Direction for Configuration 3 At the Right Side of Region 3 54
Figure 3.29 Graph of Displacement in Z Direction for Configuration 3 At the Right Side of Region 3 54
Figure 3.30 Graph of Stress Distribution for Configuration 1 At the Middle of Region 2 56
Figure 3.31 Graph of Stress Distribution for Configuration 2 At the Right Side of Region 2 57
Figure 3.32 Graph of Total Displacement for Configuration 3 At the Right Side of Region 3 57
Figure 4.1 Configuration 1 with Short Camera Holder Profile 58
Figure 4.2 Camera Holder Base Center Position 59
Figure 4.3 Exaggerated Displaced Model Shape for Short Profile 60
Figure 4.4 Exaggerated Displaced Model Shape for Long Profile 60
Figure 4.5 New Camera Holder Design 61

Figure 5.1 Dummy Camera 64
Figure 5.2 Crash Test System with the Dummy Camera 64
Figure 5.3 Off-Board Camera on the Ground 65
Figure 5.4 Off-Board Camera in front of the Catapult 65
Figure 5.5 Final Pulse Generated Before the Test 66
Figure 5.6 The Crash Test System with High-g High Speed Imaging Camera 67
Figure A.1 Camera Holder Support Arm 73
Figure A.2 Technical Drawing of the First Component 74
Figure A.3 Technical Drawing of the Second Component 74
Figure A.4 Technical Drawing of the Third Component 75
Figure A.5 Technical Drawing of the Forth Component 75
Figure A.6 Camera Holder Arm 76
Figure A.7 Technical Drawing of Camera Holder Arm 76
Figure A.8 Technical Drawing of Camera Holder Profile 77
Figure A.9 Camera Holder 78
Figure A.10 Technical Drawing of the First Component of Camera Holder 78
Figure A.11 Technical Drawing of the Second Component of Camera Holder 79
Figure A.12 Technical Drawing of the Second Component of Camera Holder 79
Figure A.13 Technical Drawing of the Second Component of Camera Holder 80

LIST OF SYMBOLS

SYMBOLS

$[C]$: Structure Damping Matrix

dV : Integrated Volume

$\{F^{EXT}\}$: Total External Forces

$\{F^{INT}\}$: Total Internal Forces

$[K]$: Stiffness Matrix

$[M]$: Structure Mass Matrix

$[N]$: Shape Function

$[N]^T$: Transpose of Shape Function

$\{u\}$: Displacement Vector

$\{u^{'}\}$: Velocity Vector

$\{u^{''}\}$: Acceleration Vector

α : Stiffness related damping coefficient

ρ : Density of Material

CHAPTER 1

INTRODUCTION

1.1 Importance of Crash Test Systems

Through more than hundred years history of cars, safety has always been a serious concern and nowadays, one of the most important elements in car sales is safety. The effect of this element in purchasing decision is becoming a key element more than ever before. Accordingly, manufacturers are showing diligent efforts to design cars more safer. Thus, although the traffic is increasing, the number of fatal accidents and serious injuries is constantly decreasing. This is the situation coming from achieving more safety in cars. The achievement of these safer cars is driven by comprehensive crash tests. Over the last years, crash-proof measuring tests have been ensuring whether the design and the equipment of the car is adequate for safety or not. A crash test can give prompt information for the behaviour of the components or systems, which otherwise can be difficult to realize. Before going to mass production, it is a must to have the product been tested in crash test systems and get a value for its resistance to real life simulated crashes. The challange for manufacturers is to offer highly sophisticated and reliable safety systems at reasonable prices. Thus, vehicle manufacturers are trying to keep the costs of safety systems within certain limits. For this purpose, crash tests are playing a very important role.

Early in the century, there were virtually no safety regulations in place. During the 1930s, the industry took notice of very high injury and fatality rates. After World War II, action was taken to begin making cars safer. A major emphasis was on reducing injuries incurred during accident [1]. Crash test systems have contributed greatly to identifying ways of making cars safer. Regulations also played an

important role in improving safety of automobiles. So, at the current stage for every new design, the manufacturer should make crash tests according to the standarts and the designs should get an adequate value to pass from these crash tests.

Two types of tests are used for the safety evaluation of vehicles. One of them is the destructive type of crash tests. On these crash tests, real cars are used and they run straight into a solid concrete barrier or to another vehicle.

The types of these crash tests are [2];

- Frontal-Impact Tests
- Offset Tests
- Side-Impact Tests
- Roll-over Tests
- Roadside Hardware Crash Tests

The other type of tests is the sled crash test which is also used at METU-BİLTİR Center Vehicle Safety Unit. This is a nondestructive test because it does not harm the vehicle during the test. Sled testing allows engineers to reproduce the dynamic conditions of a full-scale crash test in a controlled environment at a fraction of the cost [3].

There are two type of regulations that are used in the evaluation of the cars in the above tests. One is the US Regulations, the other one is the European Regulations. Under these regulations, there are a lot of different tests specialized for different parts of the vehicle. These tests are [4];

- Interior Testing
- Dash Board
- Frontal Impact
- Side Impact
- Steering Wheel
- Seats
- Seat Belts

- Rear Impact
- Rollover
- Head rests and
- Bumpers

There are slight differences in the application between US and European Regulations.

Nowadays, most popular vehicle safety rating system is Euro NCAP (European New Car Assessment Programme) which was founded in 1997. Euro NCAP publishes safety reports on new cars, and awards 'star ratings' based on the performance of the vehicles in a variety of crash tests, including front, side and pole impacts, and impacts with pedestrians. The top overall rating is five stars [5].

The technological growth and continuous developments on crash tests are helping to make the accidents less fatal and save thousands of lives.

1.2 Crash Test System at METU-BILTIR Center

The Crash Test System at METU-BILTIR Center Vehicle Safety Unit is shown in Figure 1.1 .

The type of the crash test system at METU-BILTIR Center Vehicle Safety Unit is sled type crash test system. This type is one of the most important test methods for the evaluation of vehicles or vehicle components with respect to crash safety. As explained in the previous chapter, this type also allows to simulate real crash conditions without destroying the vehicle.

Figure 1.1 Crash Test System at METU-BILTIR Center

Areas of application of the crash simulation system [6]:

- Dynamic seat testing to ECE-R17, ECE-R80
- Dynamic seat testing to AS 8049(Aerospace Standard)
- Crash simulation tests with dummies in the vehicle body or on a rigid fixture
- Dynamic testing of restraint systems to ECE-R16
- Crash Simulation tests with pyrotechnical restraint systems (belt retractors, airbags)
- Testing of cargo restraint systems to DIN 75410/2
- Child seat testing to ECE R-44
- Low speed rear end impact - seat testing

- Test pulses to US and Euro NCAP

Before the crash test, the test sample is mounted on the sled. During the crash test, firstly the sled is accelerated within typically approximately 100 ms to the desired impact load and then smoothly decelerated. The sled acceleration is accomplished by catapult actuator unit. The catapult actuator unit is composed from 6 cylinders. In these cylinders there are pistons. Nitrogen exists in one side of the piston and the other side is filled with oil during the test. The oil in the cylinders pressurizes the nitrogen and after some point the pressurized nitrogen starts to move the oil thorugh the valves in the cylinders. The flow of this oil is determined according to the test pulse and the ram starts to move. The ram pushes the sled according to the test pulse.

The system uses a hydraulically actuated friction brake acting directly against the sled in order to decelerate the sled. The hydraulic system used at METU-BİLTİR Center Vehicle Safety Unit is shown in Figure 1.2.

In some crash tests, it is needed to use crash test dummies. Crash test dummies are the key element as they are used as replica for man in a crash test. In today tests, Hybrid III dummies shown in Figure 1.3 are the standard for the car crash test industry. The Hybrid III Dummy family consists of a small adult (5th percentile) female dummy, a midsized adult (50th percentile) male dummy, a large adult (95th percentile male dummy), and 3-year-old and 6-year-old child dummy [7].

For the successful record of the data during the crash test, Kayser Threde Advanced Data Acquisition System is used. The data acquisition system gets measurements from the accelerometers, strain gauges, pressure transducers on the test system within a lot of channels. The performance of the data acquisition system plays a crucial role for the success of the crash tests. SAE J211 and ISO 6487 are the similar documents published by the two standards organizations and are the main specification documents governing the performance requirements of crash test data acquisition

systems [8]. The data acquisition system used at METU-BİLTİR Center Vehicle Safety Unit is shown in Figure 1.4.

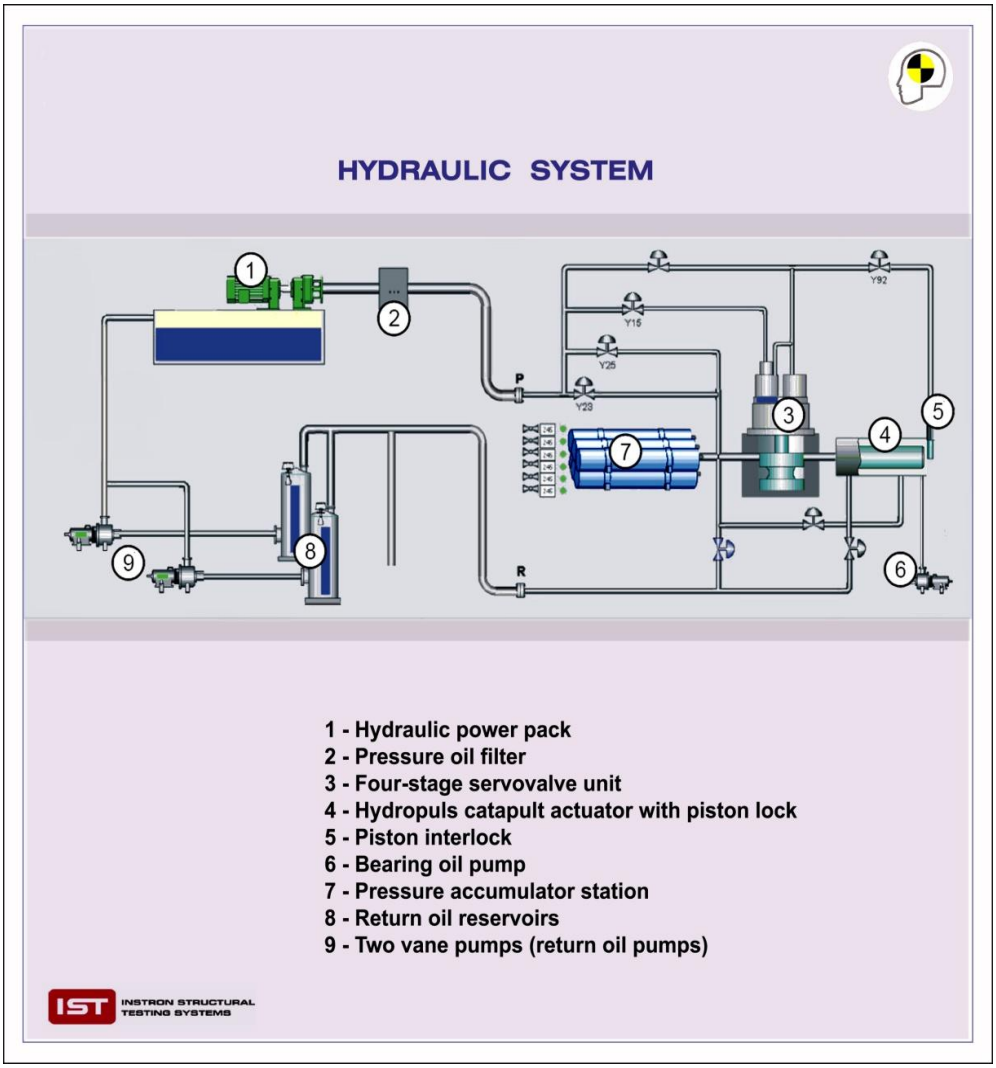

Figure 1.2 Hydraulic System Schematic of Catapult System

All the scenario of the crash test is recorded with high-g high speed imaging cameras. The importance of high-g high speed imaging cameras is summarized in Section 1.3.

Figure 1.3 Test Dummies Family

Figure 1.4 Minidau Advanced with 32 Channels

For the successful investigation of the high speed imaging during a crash test, quantity and quality of light is very important. If sufficient light is not satisfied during crash test, the visual data acquired by the high speed cameras will not be valuable. When the camera speed increases, the necessary amount of light should increase [9]. Thus, appropriate lighting solutions are needed for crash test systems.

At METU-BİLTİR Center Vehicle Safety Unit, high intensity lights are used with computerized controls as shown in Figure 1.5. By this way, the systems is presenting strong and consistent lighting solutions to the high speed cameras. There are also two mobile and two onboard lighting solutions at the METU-BİLTİR Center Vehicle Safety Unit. These lighting solutions are used for focusing on some parts of the test sample in detail.

-

Figure 1.5 Lighting System

1.3 High Speed Imaging

Rapid events, such as a crash, occur too quickly for the human eye to take everything that happens in detail. Although it may be possible to measure various parameters in many cases, the ability to visually follow the event often provides important additional information. Thus, when action occurs too quickly for the human eye to detect it, high-speed video cameras are invaluable. High speed cameras and video systems are used worldwide in demanding environments where accurate high speed recordings should be taken.

In crash tests high speed cameras can record the details of impacts and provide in-depth visual insights into events that happen during crashes. Crash tests take only a few hundred milliseconds. This means that it only takes miliseconds from the first contact until the vehicle or the sled comes to complete standstill. In order to make this short event visible and investigatable for the engineers it is necessary to use high speed cameras. These cameras take 1000 or more pictures per second (this is very fast compared to a standard video camera that only takes 25 pictures per second) [10].

In the case of crash tests, car crash testers want to see how the systems and their components perform, and also see the movements of the crash dummy or dummies. Related with this aim, filming the event with a high-speed camera means that it can subsequently be seen in slow motion and analysed step by step.

There are two types of high-g high speed cameras used at METU-BİLTİR Center Vehicle Safety Unit.

One of them is Visario G2 camera shown in Figure 1.6. It records the action in different frames according to the resolution of the record.

- 1000 fps with 1536x1024 Resolution
- 2000 fps with 1024x768 Resolution

Figure 1.6 Visario G2 High Speed Camera

The other one is Speedcam Minivis camera shown in Figure 1.7. It records the action in 500 fps with 1280x1024 resolution.

Figure 1.7 Visario G2 High Speed Camera

In order to acquire successful recording, it is very important to secure the camera on the sled crash test system satisfactorily. Since during the crash test, there occur large forces in miliseconds, the camera support structure must withstand these forces and hold the camera as strong as needed. Only by this way, good investigation of the crash test can be achieved.

To sum up, high speed imaging plays a crucial role in the success of result evaluation from the crash test and in order to have good investigation the camera support structure should be strong enough to hold the camera in place.

1.4 The Camera Support Structure at METU-BİLTİR Center Vehicle Safety Unit

During the crash test, high values of acceleration are applied to the crash test system. As explained in Section 1.3, high-g high speed cameras are used in order to record the test event satisfactorily. These high-g high speed cameras should be well secured to the sled crash test system to withstand to the high loads experienced during the sled crash test. Therefore, a camera support structure with three different configurations has been designed to be used during these tests at METU-BİLTİR Center Vehicle Safety Unit. These three configurations are used according to the position of the camera relative to the sled. Configuration 1, Configuration 2 and Configuration 3 are shown in Figure 1.8, Figure 1.9 and Figure 1.10 respectively. The detailed explanation for the components of the camera support structure will be given in Chapter 4.

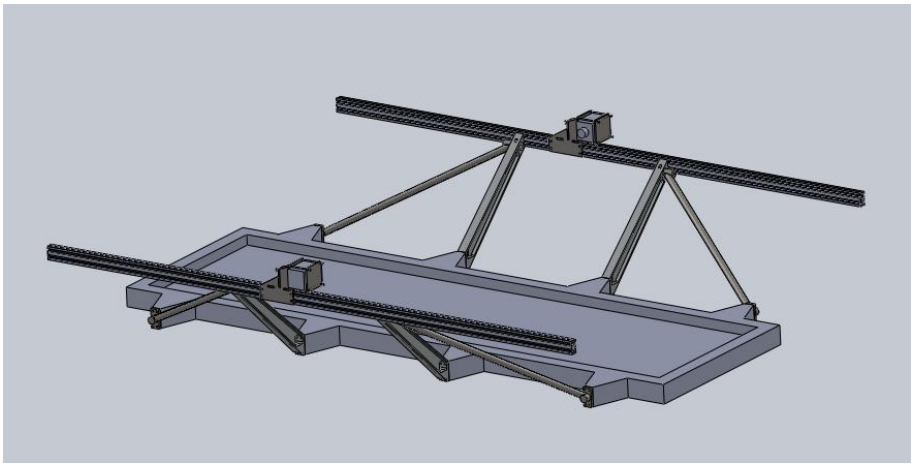

Figure 1.8 Configuration 1 of Camera Support Structure

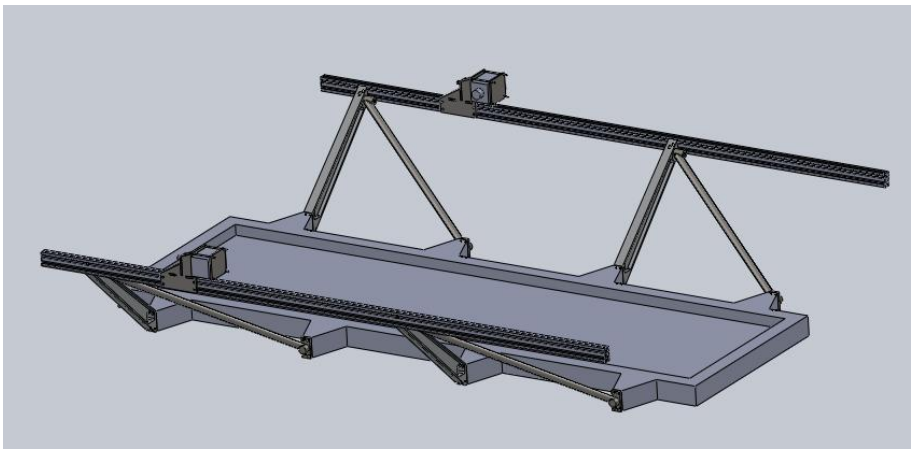

Figure 1.9 Configuration 2 of Camera Support Structure

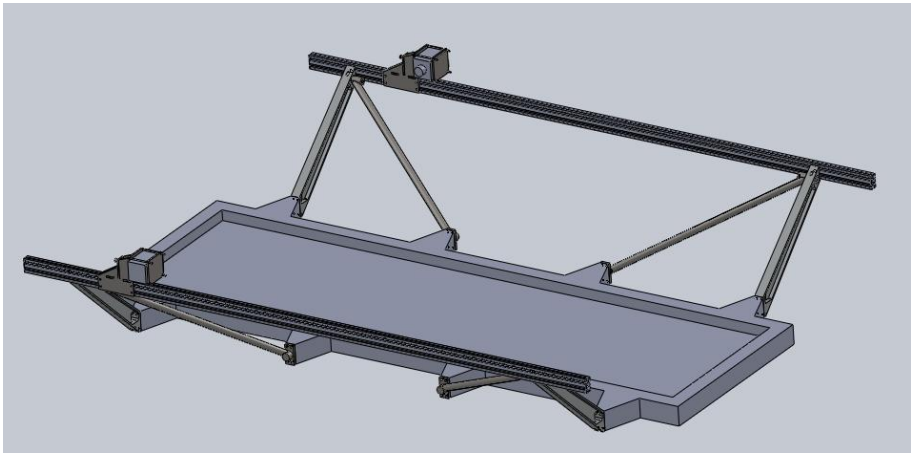

Figure 1.10 Configuration 3 of Camera Support Structure

1.5 Scope of the Thesis

In the previous sections, necessity of the usage of the camera support structure to secure high-g high speed camera to the sled crash test system has been discussed. In this study, structural analysis of three different configuration of the camera support structure available at METU-BİLTİR Center Vehicle Safety Unit will be examined under the loading with 90 g acceleration which is the maximum applicable acceleration on the system. By this way, the configurations of the design will be verified under the maximum applicable acceleration before actual use of the camera support structure in crash tests. The configuration of the camera support structure

design that should be used according to the location of the camera holder relative to the sled will be determined. After the verification with computer simulations, the crash simulation on the sled crash test system will be performed.

In Chapter 2, Finite Element Method for Transient Dynamic Analyses will be summarized. The comparison of solution methods used in this type of analyses will be also discussed in this chapter. Furthermore, the inputs and parameters of the computer simulations for the camera support structure are explained and in Chapter 3 computer simulations and results will be presented

In Chapter 4, an alternative camera holder profile and camera holder design will be discussed.

In Chapter 5, test procedure and the test result will be explained.

Finally, in Chapter 6, conclusions and suggestions for future works will be given.

CHAPTER 2

TRANSIENT DYNAMIC FINITE ELEMENT ANALYSIS FOR THE CAMERA SUPPORT STRUCTURE

As explained in Chapter 1, for the secure connection of the high-g high speed cameras, camera support structure is used. The camera support structure at METU-BİLTİR Center Vehicle Safety Unit can be assembled in three different configurations. In this study, the transient dynamic analysis of these three different configurations of the camera support structure with different camera position cases will be made. For all of the configurations, the same acceleration enforced motion graphics will be applied with the maximum acceleration value of 90 g which is the maximum applicable acceleration on the system. The details of configurations of the camera support structure and the inputs and parameters of the computer simulations are given in the following sections.

2.1 Configurations of the Camera Support Structure

The camera support structure system is composed of the same components for all of the configurations as seen in Figures 2.1 – 2.3. Two identical camera support structures are fixed to the sled. One is used to record the crash test from the left hand side of the sled crash test system, the other one is used to record from the right hand side of the sled crash test system. Configuration 1, Configuration 2 and Configuration 3 are shown in Figure 2.1, Figure 2.2 and Figure 2.3 respectively.

Assembly of the camera support structure is realized according to the following order;

1- Camera holder arms are fixed to the sled.

2- Camera holder support arms are fixed to the sled and the camera holder arms.
3- The camera holder is fixed to the camera holder profile.
4- The camera holder profile together with the camera holder is fixed to the upper ends of the camera holder arms.
5- The high-g high speed camera is clamped between the plates of the camera holder.

The components composing these configurations will be explained in the following sub-sections.

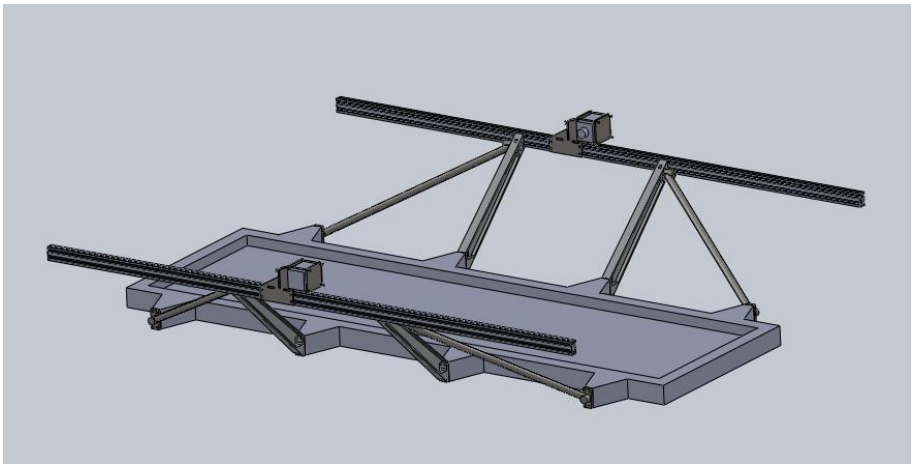

Figure 2.1 Configuration 1 of Camera Support Structure

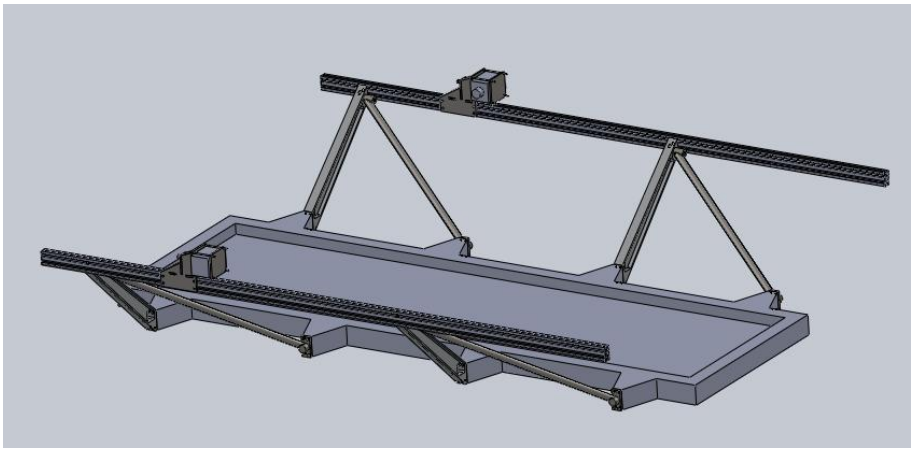

Figure 2.2 Configuration 2 of Camera Support Structure

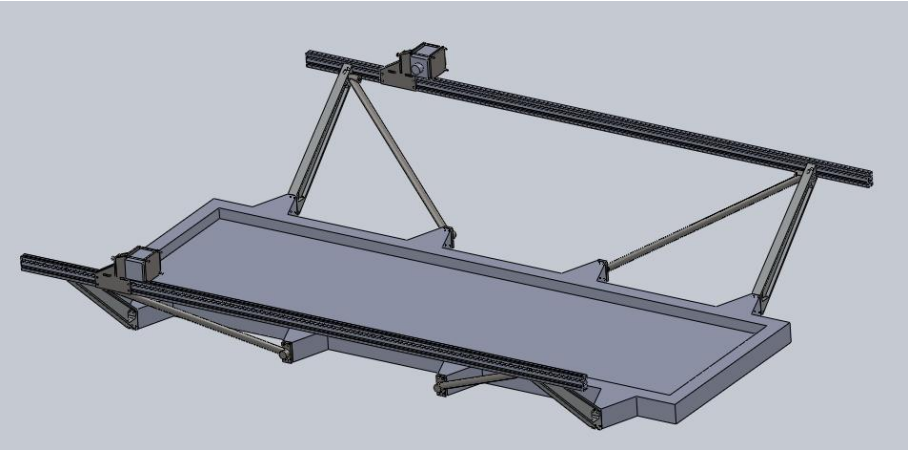

Figure 2.3 Configuration 3 of Camera Support Structure

2.1.1 Sled

Sled is the main part of the system on which the camera holder arms and camera holder support arms are fixed and the sled is shown in Figure 2.4. There are securing locations on the right and left side of the sled as shown in Figure 2.4.

Figure 2.4 Sled of the Crash Test System

2.1.2 Camera Holder Arms

The camera holder arm is shown in Figure 2.5. There are two camera holder arms used at each side of the system. All of the camera holder arm designs are same, but

only the places where they are fixed are different from each other. The places of the camera holder arms on the sled make up different configurations shown in Figures 3.1 – 3.3. The camera holder arms are fixed to each side of the sled by using M10 screws as shown in Figure 2.6.

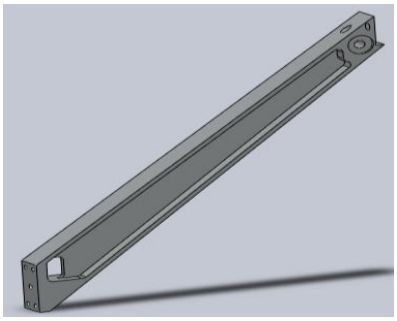

Figure 2.5 Camera Holder Arm

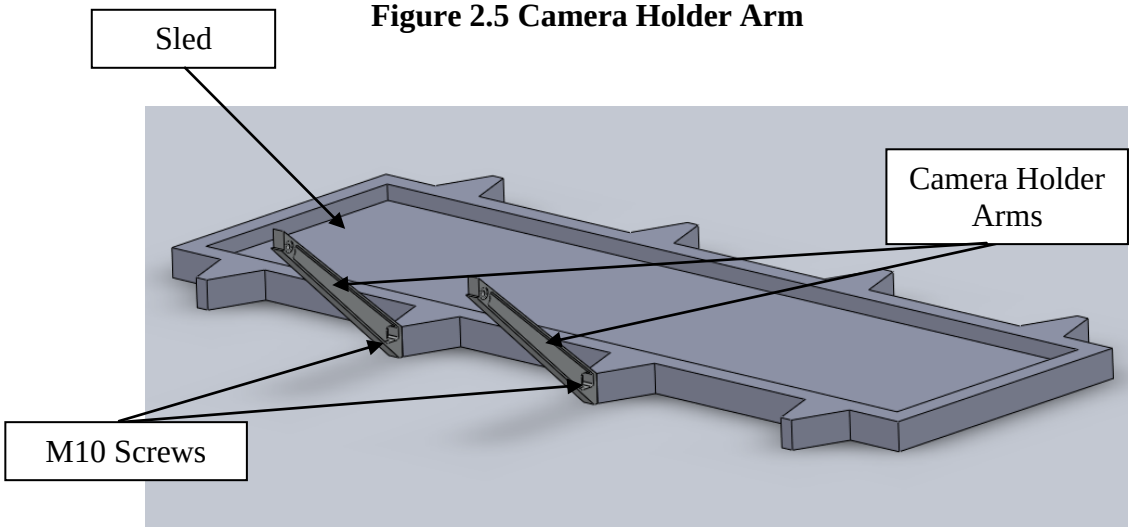

Figure 2.6 Assembly of the Camera Holder Arms with the Sled

2.1.3 Camera Holder Support Arms

In order to support the camera holder arms, the camera holder support arms shown in Figure 2.7 are used. Firstly, the camera holder support arms are fixed to the sled by using M10 screws. Afterwards, in order to enhance the structural strength of the camera holder arms during the crash tests, camera holder support arms are secured to the camera holder arms by using M20 screws as shown in Figure 2.8.

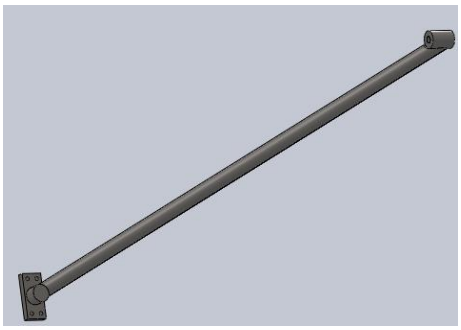

Figure 2.7 Camera Holder Support Arm

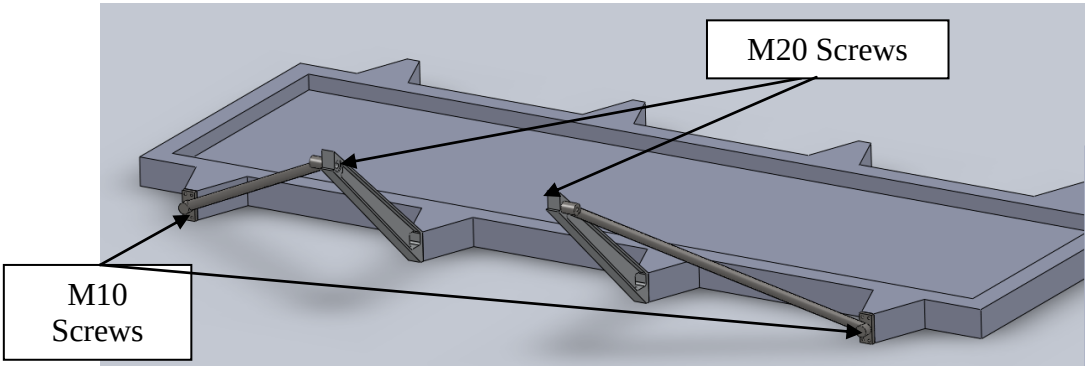

Figure 2.8 Assembly of the Camera Holder Support Arms to the Sled and the Camera Holder Arms

2.1.4 Camera Holder

The camera holder is shown in Figure 2.9. This is the main part that holds the camera in the structure. Camera is clamped within two plates by means of four M8 bolt and nut connections. Before attaching camera to the camera holder, the camera holder is secured to the camera holder profile by using M8 screws.

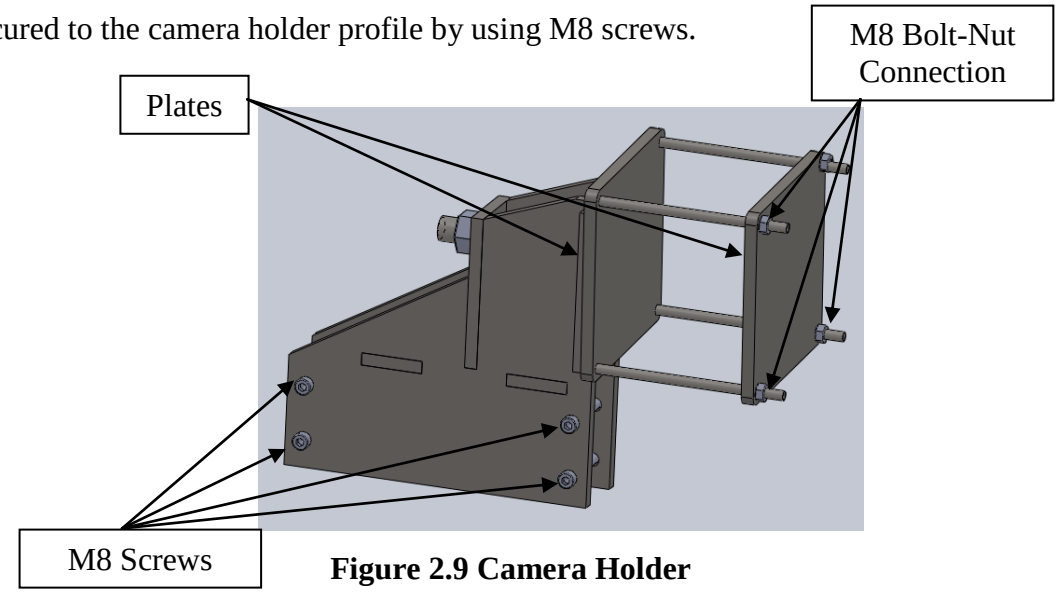

Figure 2.9 Camera Holder

2.1.5 Camera Holder Profile

The camera holder profile is shown in Figure 2.10.

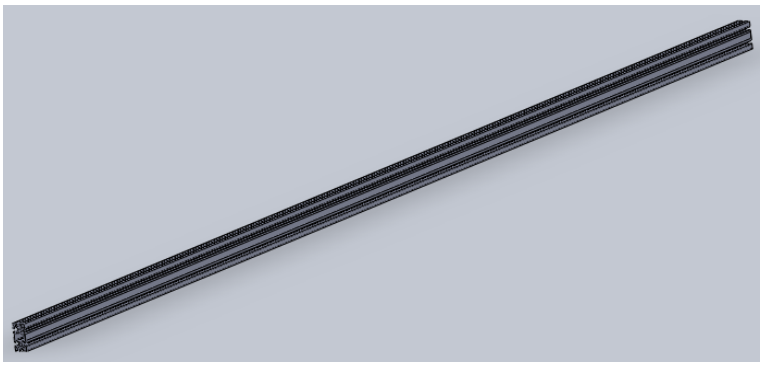

Figure 2.10 Camera Holder Profile

The camera holder profile is a standard structural member with the 2D cross section shown in Figure 2.11.

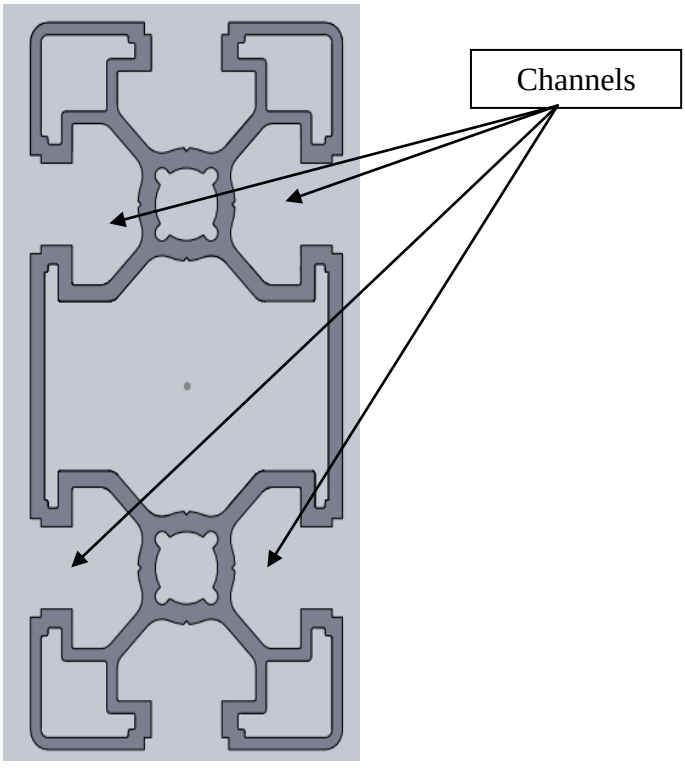

Figure 2.11 Camera Holder Profile Cross Section

Camera holder is secured to the camera holder profile as shown in Figure 2.12. Camera holder can slide on the profile channels shown in Figure 2.11 and by this way it is possible to place the camera holder to the desired location easily. The camera holder profile together with the camera holder is fixed to the camera holder arms as shown in Figure 2.13 by using M20 screws.

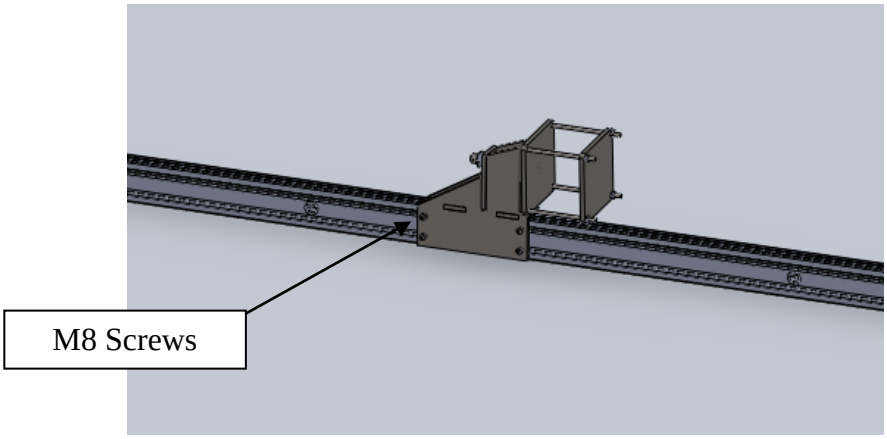

Figure 2.12 Assembly of the Camera Holder with the Camera Holder Profile

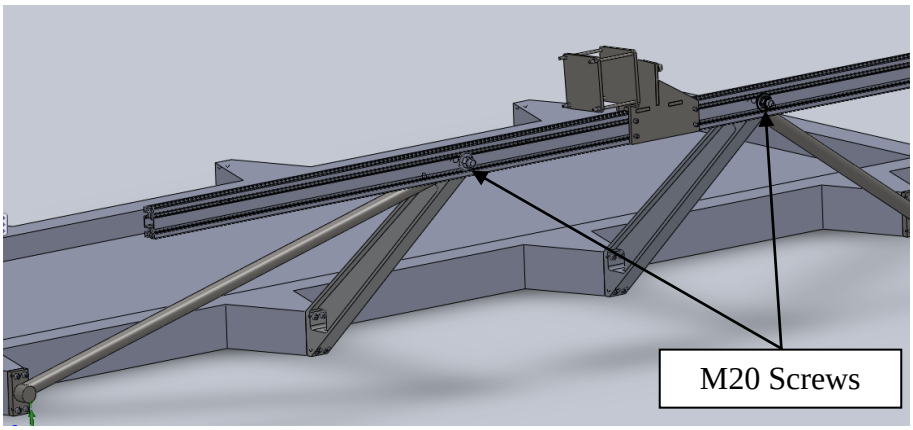

Figure 2.13 Assembly of the Camera Holder with the Camera Holder Profile

Finally, the high-g high speed camera is attached to the camera holder. After achieving the desired position by sliding the camera holder together with the camera on the camera holder profile, the camera holder is fixed to the camera holder profile by tightening the M8 screws shown in Figure 2.14.

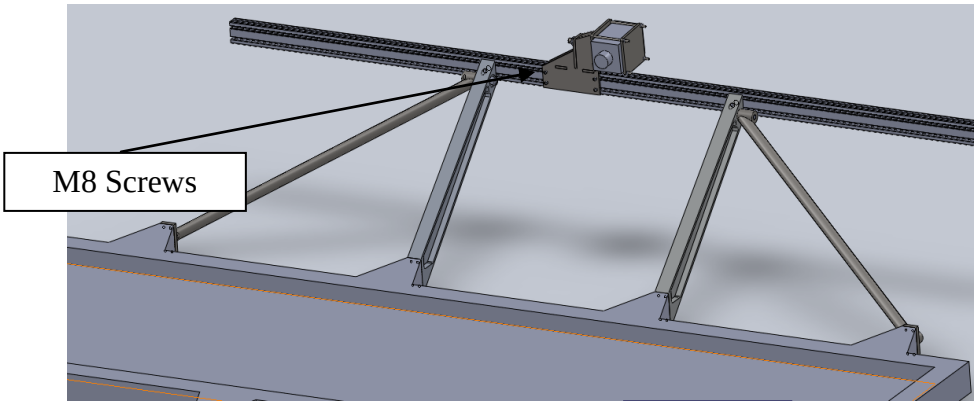

Figure 2.14 Assembled Camera Support Structure

2.2 Finite Element Method for Transient Dynamic Structural Analysis

In this study, acceleration values as high as 90 g are applied to the camera support structure system in very short time periods and transient dynamic analysis is suitable for this type of problems. With transient dynamic analysis, it is possible to see the dynamic response of a system under varying loads. These types of problems are sometimes named as time history problems.

There are two methods named as Modal Method or Direct Integration Method for the solution of transient dynamic analysis. Modal Method uses the results of a natural frequency (modal) analysis. Therefore, the natural frequency (modal) analysis needs to include enough modes to cover the contribution of the applied loads [11]. Direct Integration uses step-by-step time integration algorithms to solve the equations of motion. This method is better suited than Modal Method when shock-type loads are applied to the model.

Since a shock load is applied in short time duration in high values in this study, Direct Integration Method will be utilized for the analyses.

2.2.1 Equation of Motion

Dynamic behavior of a structure can only be described by using system of partial differential equations. In this study, these equations are solved by means of finite element method. The formula for these equations can be written as follows [12]:

$$[M]\{u''\} + [C]\{u'\} + \{F^{INT}\} = \{F^{EXT}\} \tag{2.1}$$

where;

$[M]$: Structure Mass Matrix

$[C]$: Structure Damping Matrix

$\{u''\}$: Acceleration Vector

$\{u'\}$: Velocity Vector

$\{F^{INT}\}$: Total Internal Forces

$\{F^{EXT}\}$: Total External Forces

The equation above is also known as finite element semidiscretization. It represents a system with second order ordinary differential equations changing in time.

If we have linear elastic material model, then the internal forces can be represented by;

$$\{F^{INT}\} = [K]\{u\} \tag{2.2}$$

So we have;

$$[M]\{u''\} + [C]\{u'\} + [K]\{u\} = \{F^{EXT}\} \tag{2.3}$$

where:

$[K]$: Stiffness Matrix

$\{u\}$: Displacement Vector

2.2.2 Mass Matrix

The mass distribution within a system can be expressed by a mass matrix $[M]$. There are two formulations for the representation of mass matrix.

i. Consistent Mass Matrix: The consistent mass matrix is constructed using the interpolation function used to describe the displacement field and is thus consistent with that of the stiffness matrix [13].
ii. Lumped Mass Matrix: In each node of the system, mass is represented by a particle mass m_i and summation of these particle masses, $\sum m_i$, represents the total mass of the system.

The lumped mass matrix is in the form of diagonal nature, while it is not same for consistent mass matrix. The advantage of having diagonal mass matrix in an eigenvalue analysis is the ease and reduction of computational effort as well as requirement of lesser storage space. However, it is a general belief that consistent mass matrix leads to more accurate solution. In spite of this, diagonal or lumped mass matrices are employed extensively because of the lesser computational effort it requires and the use of efficient time integration schemes, such as the explicit method of analysis [13].

In order to create a lumping mass matrix, two approaches are used. These are mass lumping and HRZ lumping scheme.

The idea in HRZ method is to use only the diagonal terms of the consistent mass matrix, but to scale them in such a way that the total mass of the element is preserved.

The diagonal matrix formed by this method is known to show good results for flexural and low order element problems. On the other hand, it gives less accurate

results for higher order plane element problems where transient analysis is required. Therefore, for the transient problem of this study mass lumping method is used.

In mass lumping, appropriate quadrature rule is applied to the following equation;

$$\int \rho[N]^T[N]dV \tag{2.4}$$

where:

ρ: Density of Material

$[N]$: Shape Function

$[N]^T$: Transpose of Shape Function

dV: Integrated Volume

2.2.3 Damping of the System

Mainly viscous damping is used for representation of the damping characteristics of the system due to its ability in approximating real damping sufficiently.

Rayleigh method is the preferred damping scheme used and it consists of a linear combination of the stiffness matrix and mass matrix.

In this study, an enforced motion within a very short period of time is utilized and the motion is accomplished directly on the total system. Thus, it is assumed to have zero damping on the system during the analysis.

2.2.4 Direct Integration Method

The equation that will be utilized for the solution of the problem is as follows:

$$[M]\{u''\}_m + [C]\{u'\}_m + [K]\{u\}_m = \{F^{EXT}\}_m \tag{2.5}$$

In this expression, Δt is the time increment and m denotes the m^{th} time increment of mΔt. For linear material model, as in the case of current study, [M], [C] and [K] show time dependent linear behaviour.

In the solution of Eq. 2.5, finite difference approximation is applied to the terms $\{u''\}$ and $\{u'\}$. Thus, $\{u''\}$ and $\{u'\}$ can be calculated in terms of $\{u\}$ at various time instants. As a result, the above equation can be expressed in terms of only $\{u\}$ terms.

For the solution of only $\{u\}$ dependent equation, there are two methods, which are explicit or implicit methods. In explicit method, the displacement at the next time step is calculated with the use of the displacement value at the previous time step. On the other hand, in implicit method, in order to calculate the displacement at the next time step, we need to know the time derivative exactly at that time increment.

Implicit methods find a solution by solving an equation involving both the current state of the system and the later one [14]. Implicit methods are often the method of choice for solving ODEs (Ordinary Differential Equations), like in stiff problems. In particular when they arise from semi-discretised PDEs (Partial Differential Equations), this implicitness causes the method to become very involved compared to explicit methods [16]. Problems involving slowly varying loads without dynamic loads can be easily solved by implicit methods.
An implicit solution procedure involves inversion of the structural stiffness and multiplication with the nodal forces to determine the corresponding nodal displacements.

$$\{u\}_{m+1} = [K]^{-1}[F^{EXT}{}_{m+1}] \tag{2.7}$$

where:

$\{u\}_{m+1}$ = Displacement at time m+1
$[K]^{-1}$ = Inversion of Stiffness Matrix
$[F^{EXT}{}_{m+1}]$ = Nodal Forces at time m+1

Once the nodal displacements have been calculated, they are used to test and verify the governing equilibrium equations [15].

Explicit methods calculate the state of a system at a later time from the state of the system at the current time [14]. The explicit solution procedure relies on the summation of the internal and external forces at each node and their corresponding division by the nodal mass to find the resulting acceleration [15]. In this method no mass inversion method is used and from the values of the acceleration, displacements are calculated. Problems involving dynamic loading within short duration of time can be easily and efficiently solved by explicit methods.

In this method, lumped mass formulation is used. The simplified equation that should be solved is;

$$[M]\{u^{''}\}_{m+1} = [F^{EXT}] - [F^{INT}] \tag{2.6}$$

where:

$[M]$ = Mass Matrix

$\{u^{''}\}_{m+1}$ = Acceleration at time m+1

$[F^{EXT}]$ = Total External Forces

$[F^{INT}]$ = Total Internal Forces

In Eq. 2.6, by the use of diagonal mass matrix $[M]$, the accelarations are solved easily. Accordingly, velocities and displacements are calculated through the use of central finite differences method.

In this study, since dynamic load is applied in a short period of time, explicit method will be utilized.

2.3 Finite Element Model

In this study, there is only translational enforced motion applied to the model. Thus, 10 – Node tetrahedral elements are used in the analyses and the stress results through the thickness of the parts can be observed. 10 – Node tetrahedral elements are formulated in three-dimensional space with three degrees of freedom per node; these are the translational degrees of freedom in the X, Y and Z directions, respectively. The 10-node element is an isoperimetric element and stresses are calculated at the nodes [11]. A typical tetrahedral element with 10 – Node is shown in Figure 2.15.

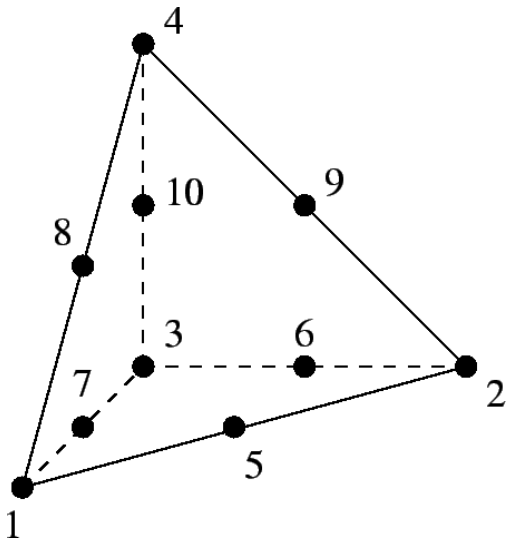

Figure 2.15 10 – Node Tetrahedral Element [11]

The Finite Element Analysis Models for Configuration 1, Configuration 2 and Configuration 3 are shown in Figure 2.16, Figure 2.17 and Figure 2.18 respectively.

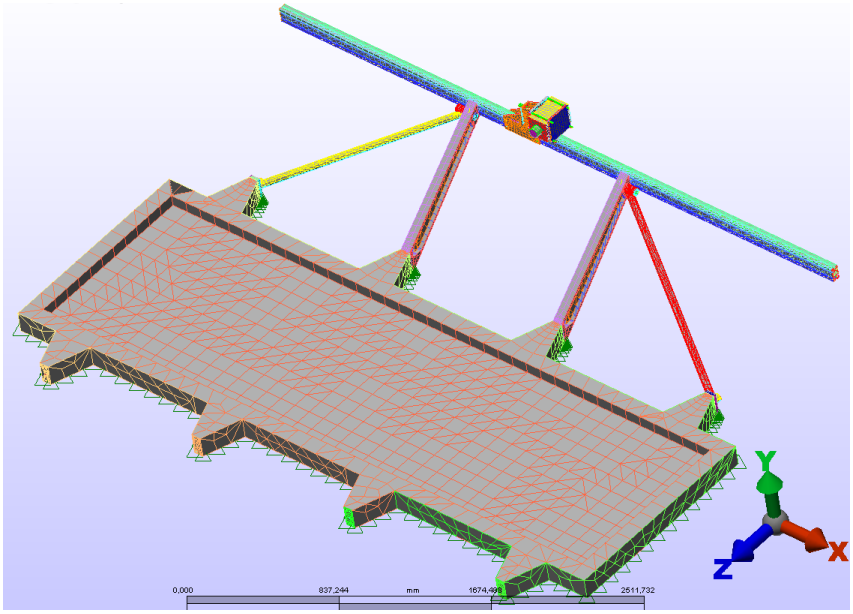

Figure 2.16 FEA Model for Configuration I

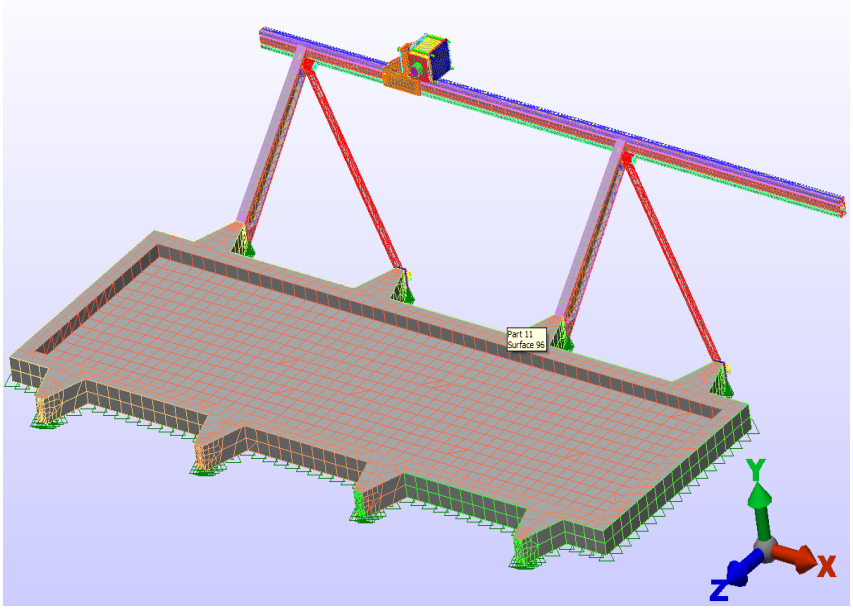

Figure 2.17 FEA Model for Configuration II

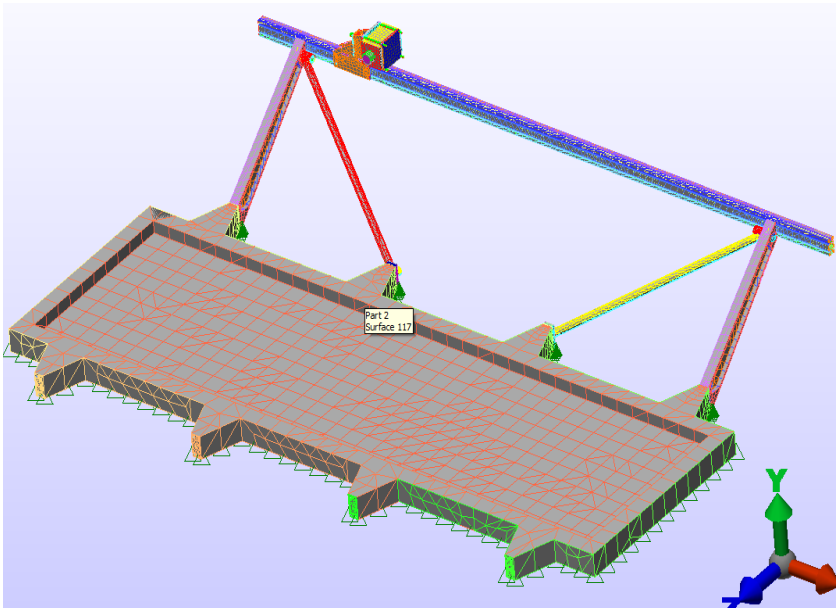

Figure 2.18 FEA Model for Configuration III

2.4 Material Properties

All parts, are made of Aluminum 6063 – T6. The material properties of Aluminum 6063 – T6 are given in Table 2.1.

Table 2.1 Material Properties of Aluminum 6063 – T6

Material Properties of Aluminum 6063 – T6		
Property	**Value**	**Units**
Elastic Modulus	69000	N/mm^2
Poisson's Ratio	0,33	NA
Shear Modulus	25800	N/mm^2
Mass Density	2.7	g/mm^3
Tensile Strength	240	N/mm^2
Yield Strength	215	N/mm^2

2.5 Bolt Connections

Most critical bolt connections are also modeled in the analyses. Preload values are selected according to the Table 2.2.

Table 2.2 Torque Values for Bolts and Screws [17]

Anma Çapı (Çap x Adım) (Nominal Diam. x Pitch)	8.8		10.9		12.9	
	Kgm.	Nm.	Kgm.	Nm.	Kgm.	Nm.
M 4 x 0.7	0.30	3	0.428	4.2	0.50	5
M 5 x 0.8	0.61	6	0.866	8.5	1.03	10.1
M 6 x 1	1.42	13	1.63	16	1.73	17
M 7	2.34	23	2.85	28	3.16	31
M 8 x 1.25	3.36	33	4.07	40	4.48	44
M 8 x 1	3.87	38	4.68	46	5.30	52
M 10 x 1.5	6.72	66	8.25	81	9.17	90
M 10 x 1.25	7.54	74	9.17	90	10.19	100
M 10 x 1	8.56	84	10.49	103	11.62	114
M 12 x 1.75	8.66	85	12.13	119	14.57	143
M 12 x 1.25	9.23	90.6	12.94	127	15.59	153
M 14 x 2	13.76	135	19.36	194	23.24	228
M 14 x 1.5	14.57	143	20.59	202	24.66	242
M 16 x 2	20.89	205	29.35	288	35.27	346
M 18 x 2.5	28.84	283	40.57	398	48.72	478
M 18 x 1.5	31.39	308	44.24	434	53.00	520
M 20 x 2.5	40.77	400	57.28	562	68.70	674

2.6 Finite Element Analysis Parameters

In this study, direction integration method with explicit solver will be utilized under acceleration type enforced motion condition since short duration impact type problem will be solved.

2.6.1 Enforced Motion Load for the Analyses

The enforced motion method is used in order to apply the load on the system. A typical deceleration curve is shown in Figure 2.19 [18]. The characteristic of this deceleration curve is used as an acceleration curve and it is simplified as shown in Figure 2.20. This simplified curve is then regenerated in order to make the maximum acceleration as 90 g which is the maximum applicable acceleration during the crash

test. In this study, this acceleration type enforced motion with a maximum value of 90 g has been applied. If the system withstands this maximum load, it means that the system can be used up to this load without problems. The graphics of applied enforced motion is shown on Figure 2.21.

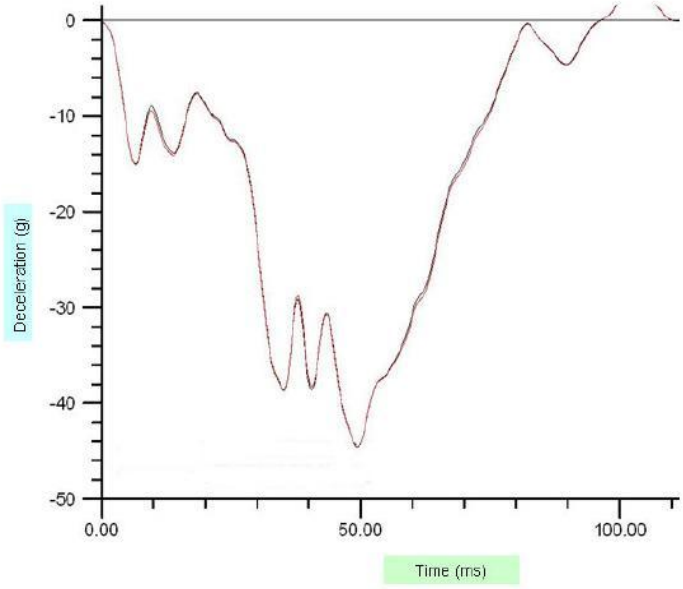

Figure 2.19 Typical Deceleration vs Time Curve [18]

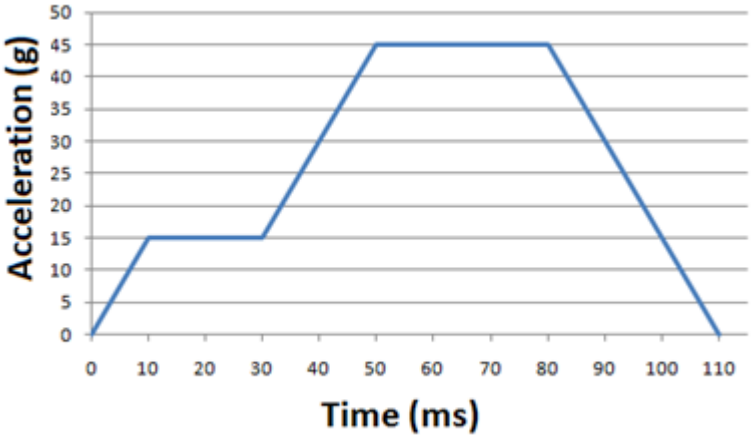

Figure 2.20 Simplified Acceleration vs Time Curve

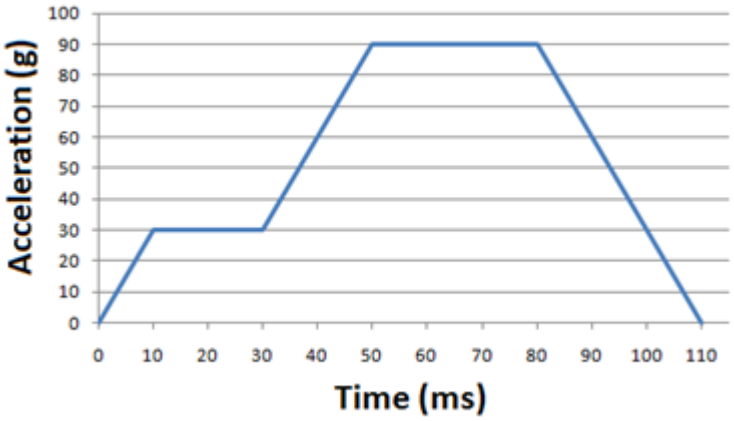

Figure 2.21 Enforced Motion Graph

The motion is applied on the sled, especially on to the bottom part of the sled since all the accelerometers are attached to the system from this part. The details are shown on Figure 2.22.

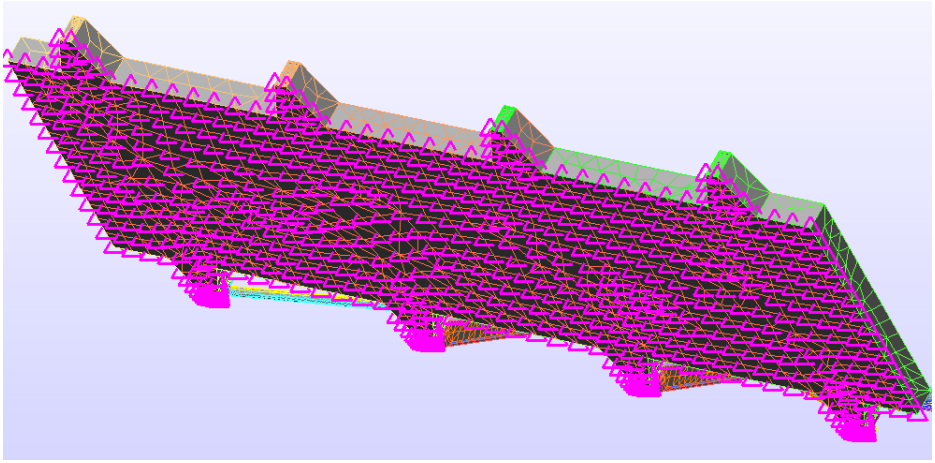

Figure 2.22 Enforced Motion Application Part

2.6.2 Time Steps and Termination Time for the Analyses

The most critical part of the test is within the time period where the acceleration motion is applied. After the enforced acceleration becomes 0, there is no need to further analyze the motion. Thus, the period that will be considered is from 0 to 110 milliseconds time period shown in Figure 2.19. If there is no problem in this period, it will imply that after this time period, there will be no problem in the system. In order to have successful analysis results, 5 milliseconds incremental time periods are

chosen. When 2,5 milliseconds time period for the analysis is chosen for the simulation of the system, there is no difference in the results. Thus, 5 milliseconds incremental time period will be adequate for the analysis.

2.6.3 Boundary Conditions

In the enforced motion type transient analysis problems, it is needed to constrain the part on which the enforced motion is applied. As mentioned in section 3.3.1, all the accelerometers are attached to the bottom part of the sled and thus the manipulated enforced motion will be according to those accelerometers. In order to simulate the test like in real life, it is needed to apply the enforced motion to the bottom of the sled. There are no other special boundary conditions required in the problem.

CHAPTER 3

COMPUTER SIMULATIONS AND RESULTS

According to the application requirement, the high speed high imaging camera may be located on different regions of the sled. These regions are named as “Region-1”, “Region-2” and “Region-3” as shown in Figure 3.1.

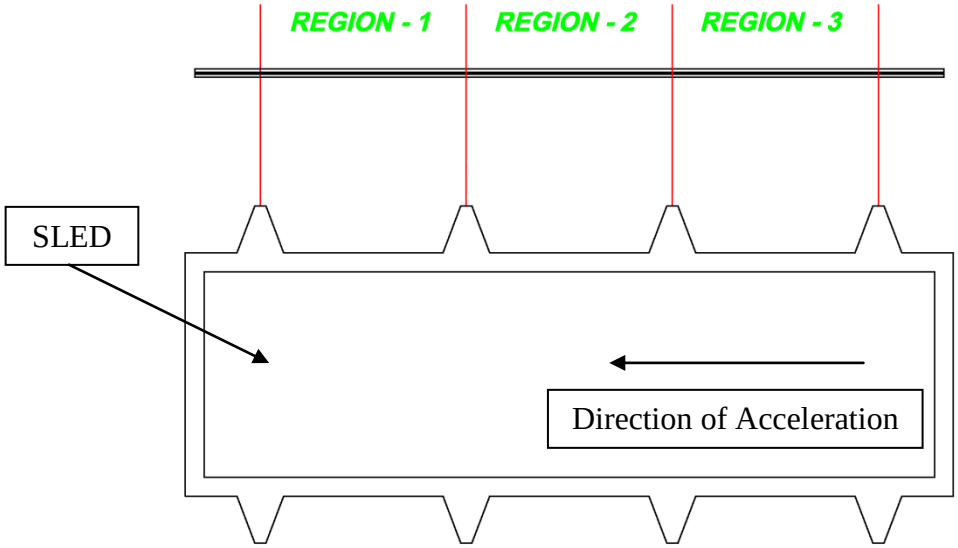

Figure 3.1 Regions for the Sled

As seen in Figure 3.1, Figure 3.2 and Figure 3.3, camera holder arms and camera holder support arms are fixed to the different positions on the sled. To see the effects of position of the camera in the regions and find the adequate configuration in the regions at the specified camera position, these three regions are further divided into three sub regions as “Left”, “Center” and “Right” as shown on Figure 3.2.

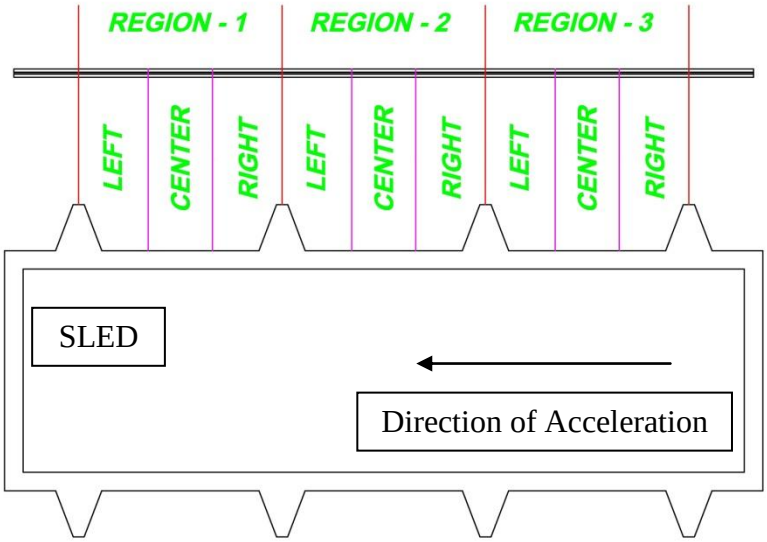

Figure 3.2 Sub-Regions for the Sled

The analyses are carried out in all of the configurations according to the position of the camera in these regions. For every configuration, there may be 9 different camera position cases that can be analyzed. For instance, right position of the camera holder in Region-1 for Configuration 1 is shown in Figure 3.3. However there is no need to analyze some of the camera position cases, because it is very obvious that the related configuration will be worse with respect to the other configurations at those position cases.

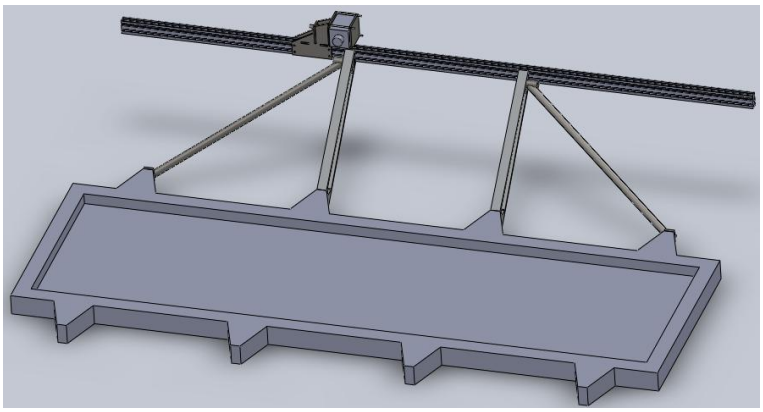

Figure 3.3 Right Position of the Camera Holder in Region-1 for Configuration 1

3.1 Results of Maximum Displacement Values of Camera Lens Center

All the displacement values are plotted at the camera lens center as shown in Figure 3.4 since high-g high speed camera records through the lens.

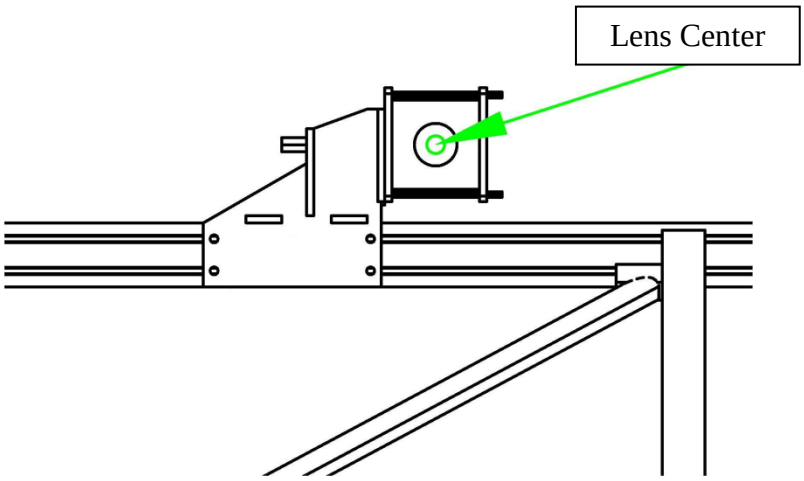

Figure 3.4 Lens Center Position of the Camera

All the displacement values are determined with respect to the axes of the camera support structure system. The axes definition of the system is shown in Figure 3.5. In the first picture the side view of the system and in the second picture, the right side view of the system is given.

The maximum total displacement values in X – Direction, Y – Direction and Z – Direction obtained on the camera lens center position shown in Figure 3.4 are tabulated in Table 3.1, 3.2 and 3.3 respectively.

Left means that the camera holder locates on the left end of the region; center means that camera holder is in the middle of the region and finally right means that camera holder is at the right end of the region.

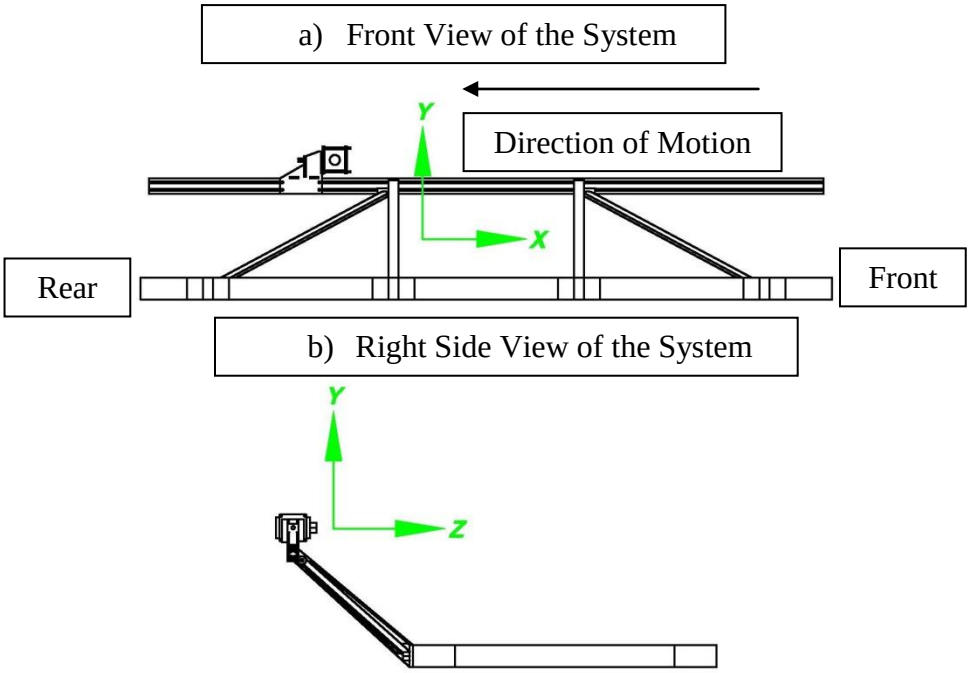

Figure 3.5 Axes Definition of the Camera Support Structure System

Table 3.1 Total Displacement Values in mm

Regions	Region-1			Region-2			Region-3		
Sub Regions	Left	Center	Right	Left	Center	Right	Left	Center	Right
Configuration - 1	*	2.10	1.75	1.50	1.40	1.70	2.20	2.80	*
Configuration - 2	1.70	1.70	1.50	1.50	1.60	1.65	2.70	2.90	*
Configuration - 3	2.10	2.15	2.10	1.75	1.60	1.65	1.75	1.80	1.62

Table 3.2 Displacement Values in X Direction in mm

Regions	Region-1			Region-2			Region-3		
Sub Regions	Left	Center	Right	Left	Center	Right	Left	Center	Right
Configuration - 1	*	1.95	1.70	1.40	1.30	1.50	1.90	2.05	*
Configuration - 2	1.55	1.50	1.40	1.45	1.50	1.60	1.90	2.20	*
Configuration - 3	1.70	1.60	1.50	1.50	1.50	1.55	1.60	1.70	1.60

Table 3.3 Displacement Values in Y Direction in mm

Regions	Region-1			Region-2			Region-3		
Sub Regions	Left	Center	Right	Left	Center	Right	Left	Center	Right
Configuration - 1	*	0.74	0.14	-0.48	-0.29	-0.47	-2.25	-3.05	*
Configuration - 2	-0.75	-0.80	-0.47	0.06	0.30	-0.23	-1.90	-3.30	*
Configuration - 3	-1.15	-1.50	-1.40	-0.90	-0.48	0.35	0.55	0.45	-0.16

Table 3.4 Displacement Values in Z Direction in mm

Regions	Region-1			Region-2			Region-3		
Sub Regions	Left	Center	Right	Left	Center	Right	Left	Center	Right
Configuration - 1	*	0.55	0.31	0.18	-0.20	-0.65	-1.22	-0.90	*
Configuration - 2	0.24	0.20	0.06	-0.33	-0.38	-0.30	-0.35	-0.60	*
Configuration - 3	0.25	0.40	0.41	0.13	-0.20	-0.38	-0.42	-0.40	-0.14

In the regions shown with *, there is no need to further make analyses for that sub regions. For Region 1, no analysis was made for the left side with Configuration 1 because it is very obvious that the displacement value will be worse than the values obtained at the center and right sides. Also since these values are worse than the values obtained for Configuration 2 and Configuration 3, it infers that the value at the left side will be worse than the value obtained for Configuration 2 and 3.

There is a similar situation at the right side of Region 3 for Configuration 1 and 2. It is very obvious that the value that will be obtained at the right side for these configurations will be worse than the value obtained in Configuration 3. Thus, there is no need to further analyze this sub region.

By observing these tabulated values for each region, one best configuration has been determined for each region.

If it is required to position the camera holder in Region 1, Configuration 2 should be used. The best place that the camera holder should be located is the right side of the Region - 1 since the displacement value obtained in this sub region is smaller than the values obtained in other two sub regions, i.e., Left and Center. The optimum

camera holder position in Region – 1 is shown in Figure 3.6. As seen in the figure, Configuration – 2 of the camera support structure is used and the camera holder is located at the right side of Region – 1.

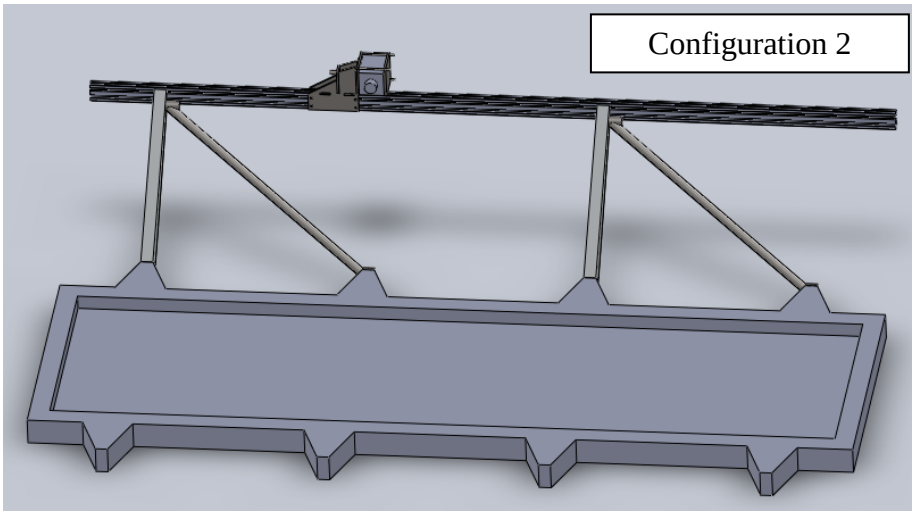

Figure 3.6 Best Configuration and Position of the Camera Holder for Region 1

If it is required to position the camera holder in Region 2, Configuration 1 should be used. The best place that the camera holder should be located is the center of the region since the displacement value obtained in this sub region is smaller than the values obtained in other two sub regions. The optimum camera holder position in this region under Configuration 1 is shown in Figure 3.7.

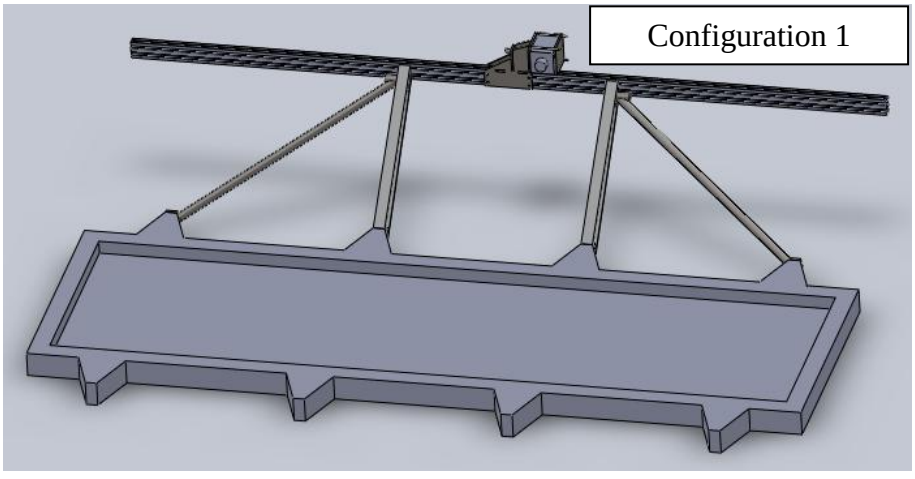

Figure 3.7 Best Configuration and Position of the Camera Holder for Region 2

Finally, if it is required to have a crash test observation in Region 3, Configuration 3 should be used. The best place that the camera holder should be located is the right side of the region since the displacement value obtained in this sub region is smaller than the values obtained in other two sub regions. The optimum camera holder position in this region under Configuration 3 is shown in Figure 3.8.

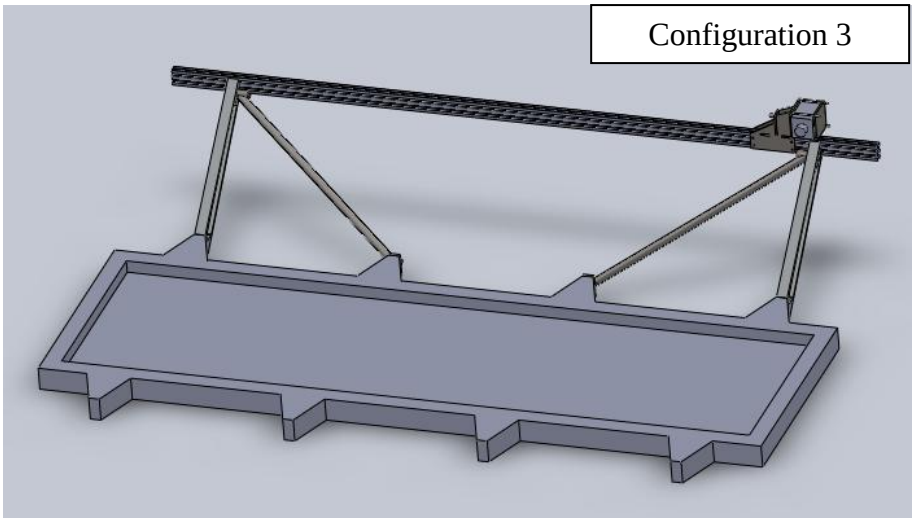

Figure 3.8 Best Configuration and Position of the Camera Holder for Region 3

According to the finite element analysis results, the recommendations for the type of configuration and the position of the camera holder that should be used in the crash test system are given in Table 3.5.

Table 3.5 Recommendations for Configuration Type and Position of the Camera Holder

Regions	Configuration	Camera Holder Position
Region – 1	Configuration - 2	Right
Region – 2	Configuration – 1	Center
Region – 3	Configuration - 3	Right

3.2 Visualization of the Displacement of Camera Lens Position

In Tables 3.1 – 3.4, the maximum values of total displacements and values of maximum displacements in X, Y and Z directions are given. According to the results of these values, one best configuration is defined for each region with the best camera holder position within the region as tabulated in Table 3.5. In this section, the exaggerated displaced model shapes for the recommended configurations with three different camera holder position cases within the region when the maximum displacements occur will be presented. By this way, it is easier to observe the behavior of the structure during the tests with different camera holder position cases in the region.

3.2.1 Displaced Model Shape of Configuration 1 in Region 2

The exaggerated displaced model of Configuration 1 in the left side of Region 2 is shown in Figure 3.9.

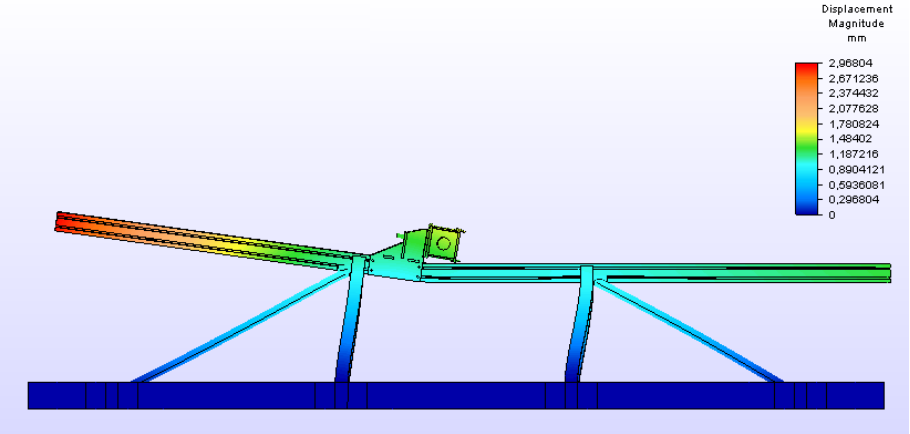

Figure 3.9 The Exaggerated Displaced Model of Configuration 1 in the Left Side of Region 2

The exaggerated displaced model of Configuration 1 in the middle of Region 2 is shown in Figure 3.10.

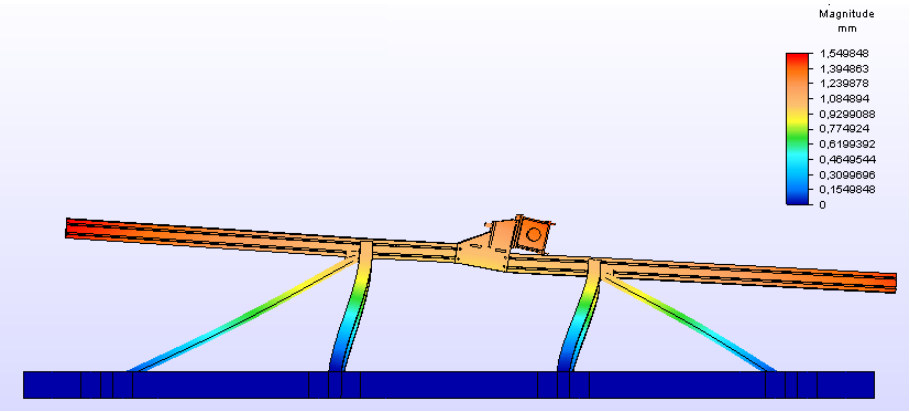

Figure 3.10 The Exaggerated Displaced Model of Configuration 1 in the Middle of Region 2

The exaggerated displaced model of Configuration 1 in the right side of Region 2 is shown in Figure 3.11.

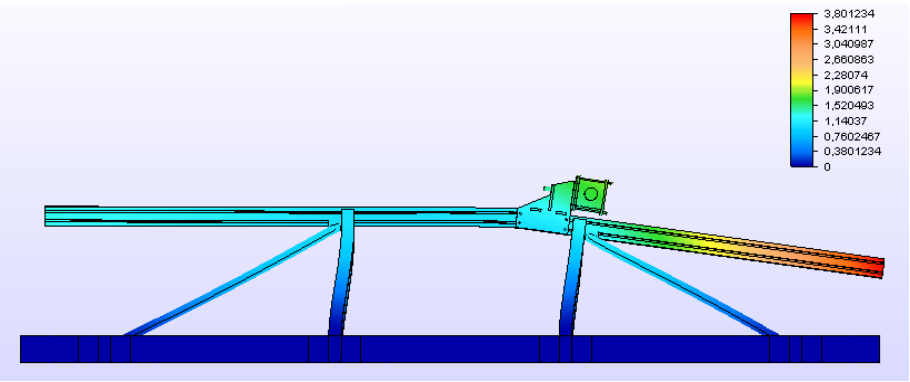

Figure 3.11 The Exaggerated Displaced Model of Configuration 1 in the Right Side of Region 2

3.2.2 Displaced Model Shape of Configuration 2 in Region 1

The exaggerated displaced model of Configuration 2 in the left side of Region 1 is shown in Figure 3.12.

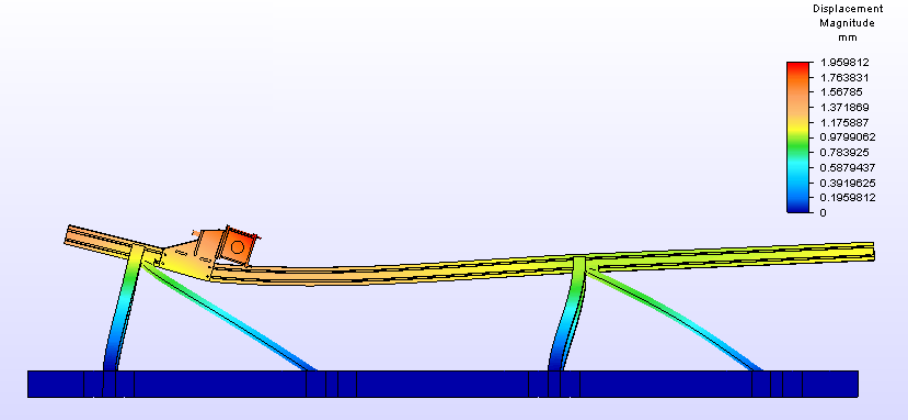

Figure 3.12 The Exaggerated Displaced Model of Configuration 2 in the Left Side of Region 1

The exaggerated displaced model of Configuration 1 in the middle of Region 2 is shown in Figure 3.13.

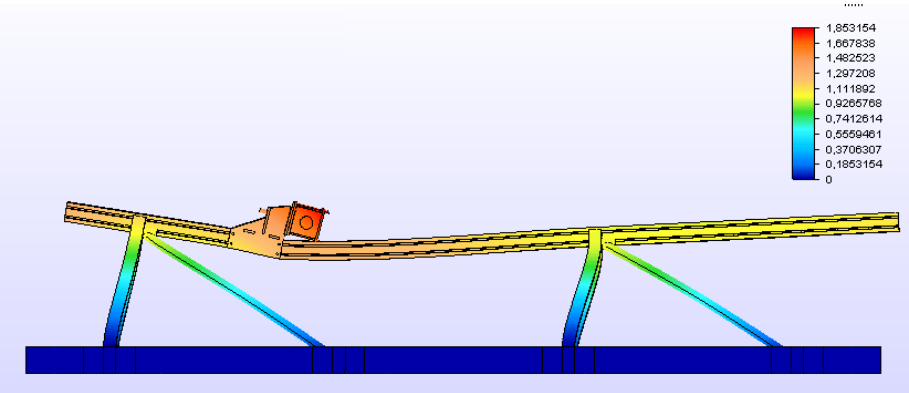

Figure 3.13 The Exaggerated Displaced Model of Configuration 1 in the Middle of Region 2

The exaggerated displaced model of Configuration 2 in the right side of Region 1 is shown in Figure 3.14.

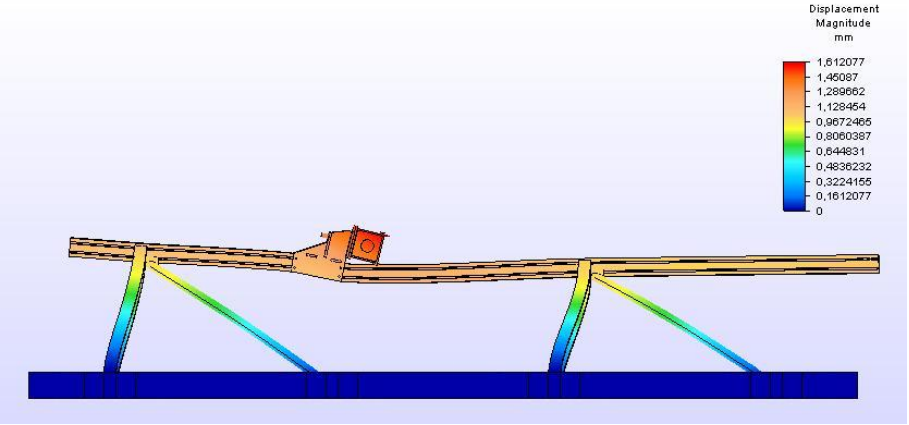

Figure 3.14 The Exaggerated Displaced Model of Configuration 1 in the Right Side of Region 2

3.2.3 Displaced Model Shape of Configuration 3 in Region 3

The exaggerated displaced model of Configuration 3 in the left side of Region 3 is shown in Figure 3.15.

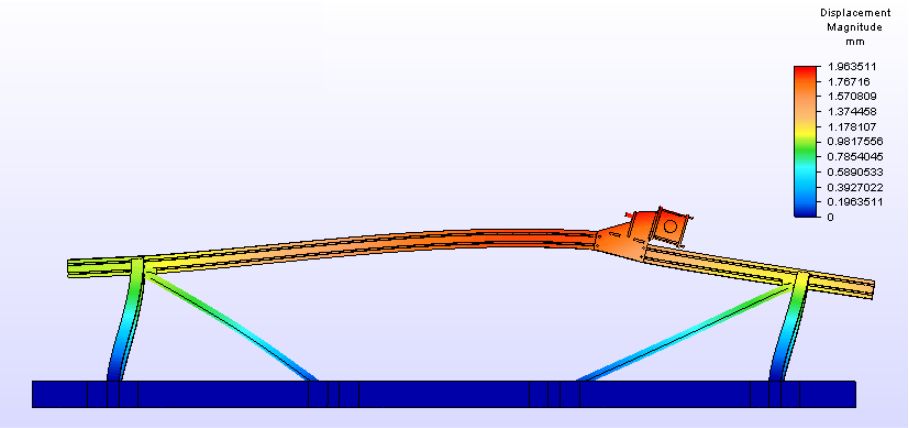

Figure 3.15 The Exaggerated Displaced Model of Configuration 3 in the Left Side of Region 3

The exaggerated displaced model of Configuration 3 in the middle of Region 3 is shown in Figure 3.16.

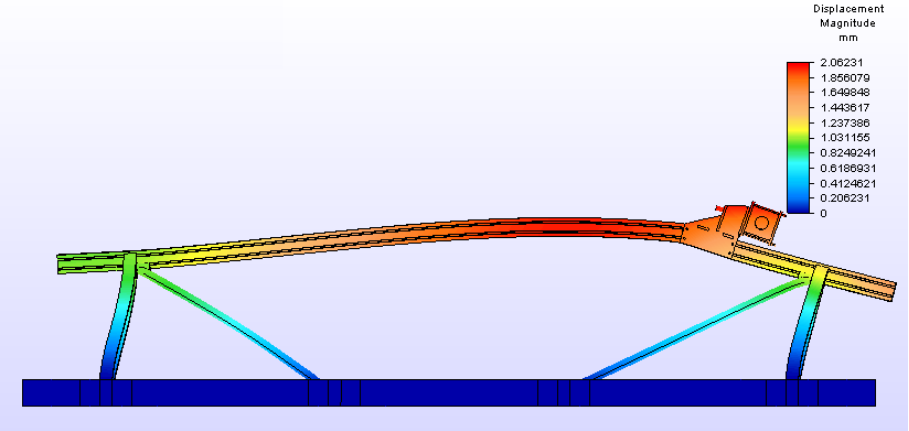

Figure 3.16 The Exaggerated Displaced Model of Configuration 3 in the Middle of Region 3

The exaggerated displaced model of Configuration 3 in the right side of Region 3 is shown in Figure 3.17.

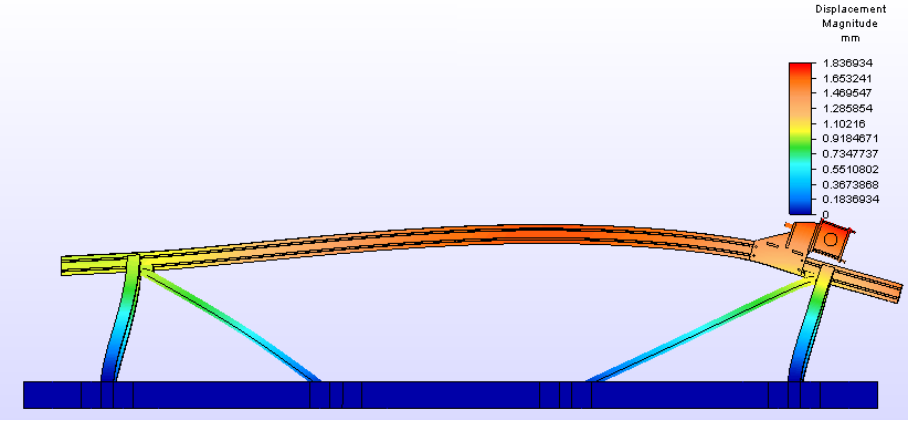

Figure 3.17 The Exaggerated Displaced Model of Configuration 3 in the Right Side of Region 3

When a sudden force is applied to the structure, the first places that react oppositely are the fixed locations. In this camera support structure, the profile is fixed to the sled by using camera holder and camera holder arms. Thus, when a sudden force is applied, these structures tend to keep their old positions and change their positions as shown in Figures 3.12 to 3.17.

The reaction of these camera holder and camera holder arms affect the behavior of other parts on the structure.

3.3 Graphical Representation for the Displacement Results of Camera Lens Position

In the Tables 3.1 – 3.4 presented previously, only the maximum values of the displacements are tabulated. In this section, the graphical time history of the displacements will be presented according to the axes definition shown in Figure 3.5.

In the analyses, it is thought that the structure does not face with vibration problems. However, it is possible to discuss the vibration characteristics of the structure by investigating the graphical time history of the displacements.

All the displacement values discussed here are plotted at the camera lens position and only the recommended configuration and camera holder position will be covered in the following sub-sections.

3.3.1 Displacement Graph for Configuration 1 at Center of Region 2

The total displacement graph for Configuration 1 when the camera holder locates at the center of Region 2 is shown in Figure 3.18. As can be observed from Figure 3.18, the maximum total displacement value for Configuration 1 when the camera holder locates at the center of Region 2 is 1,4 mm.

The displacement graph in X direction for Configuration 1 when the camera holder locates at the center of Region 2 is shown in Figure 3.19. As can be observed from

Figure 3.19, the maximum displacement value in X direction for Configuration 1 when the camera holder locates at the center of Region 2 is 1,3 mm.

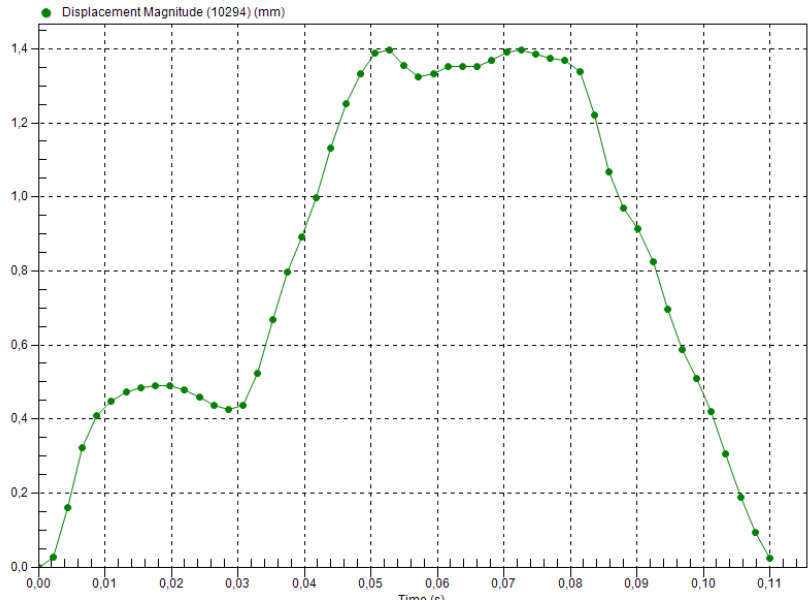

Figure 3.18 Graph of Total Displacement for Configuration 1 At the Center of Region 2

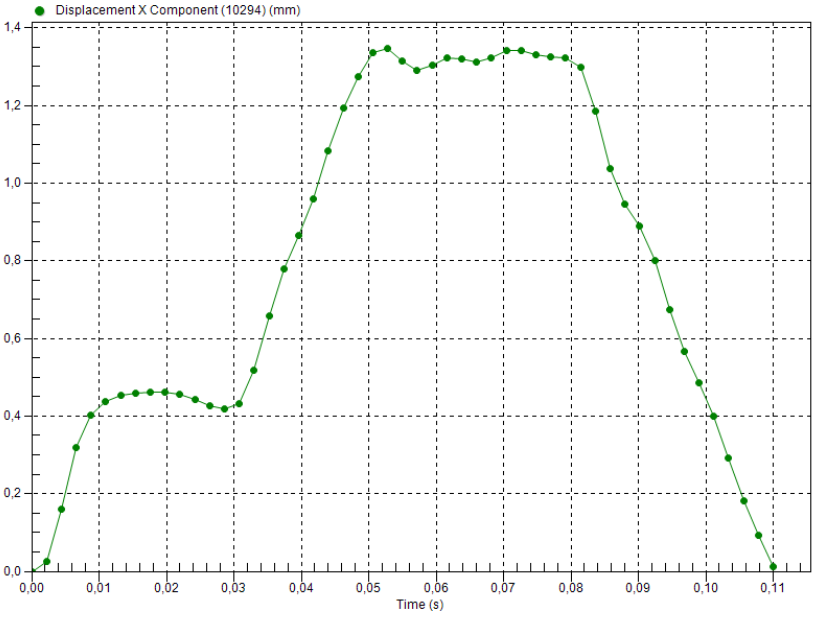

Figure 3.19 Graph of Displacement in X Direction for Configuration 1 At the Center of Region 2

The displacement graph in Y direction for Configuration 1 when the camera holder locates at the center of Region 2 is shown in Figure 3.20. As can be observed from Figure 3.20, the maximum displacement value in Y direction for Configuration 1 when the camera holder locates at the center of Region 2 is -0.31 mm.

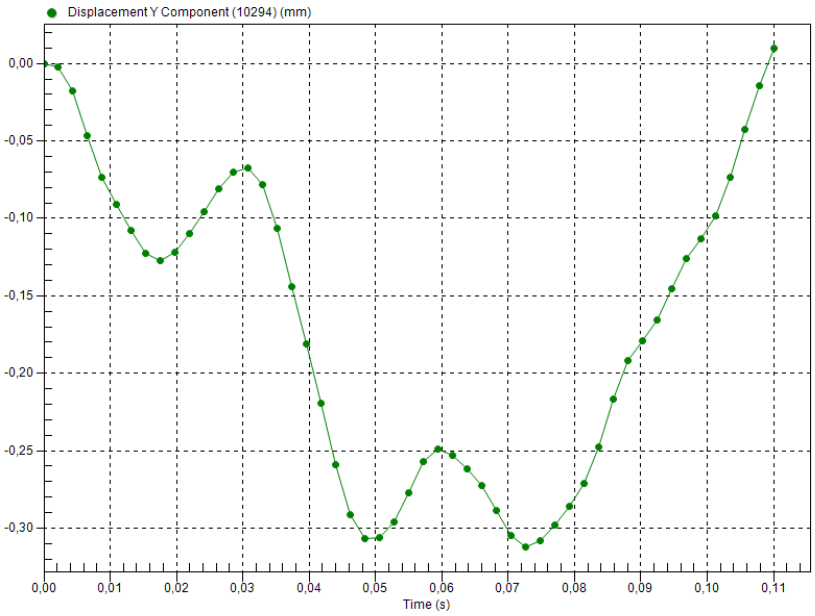

Figure 3.20 Graph of Displacement in Y Direction for Configuration 1 At the Center of Region 2

The displacement graph in Z direction for Configuration 1 when the camera holder locates at the center of Region 2 is shown in Figure 3.21. As can be observed from Figure 3.21, the maximum displacement value in Z direction for Configuration 1 when the camera holder locates at the center of Region 2 is -0.24 mm.

3.3.2 Displacement Graph for Configuration 2 at the Right Side of Region 1

The total displacement graph for Configuration 2 when the camera holder locates at the right side of Region 1 is shown in Figure 3.22.

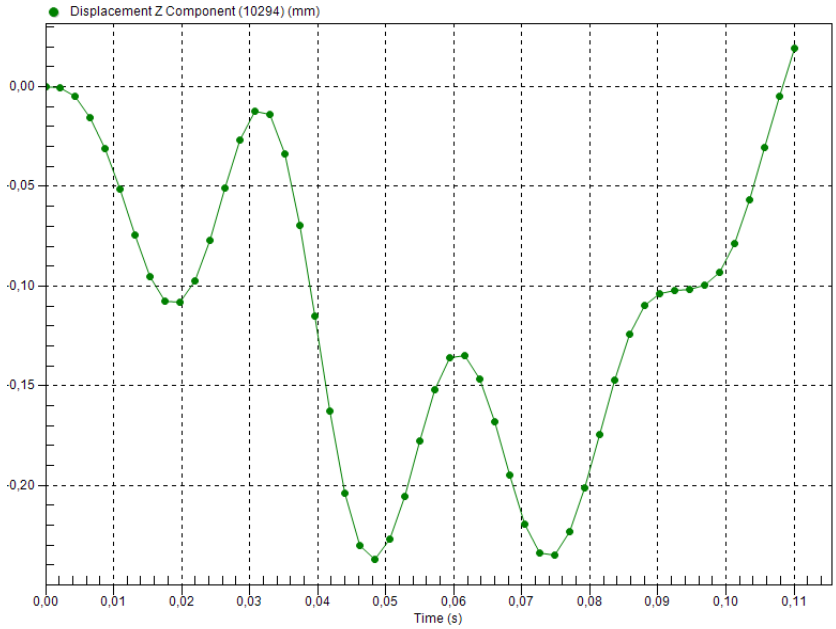

Figure 3.21 Graph of Displacement in Z Direction for Configuration 1 At the Center of Region 2

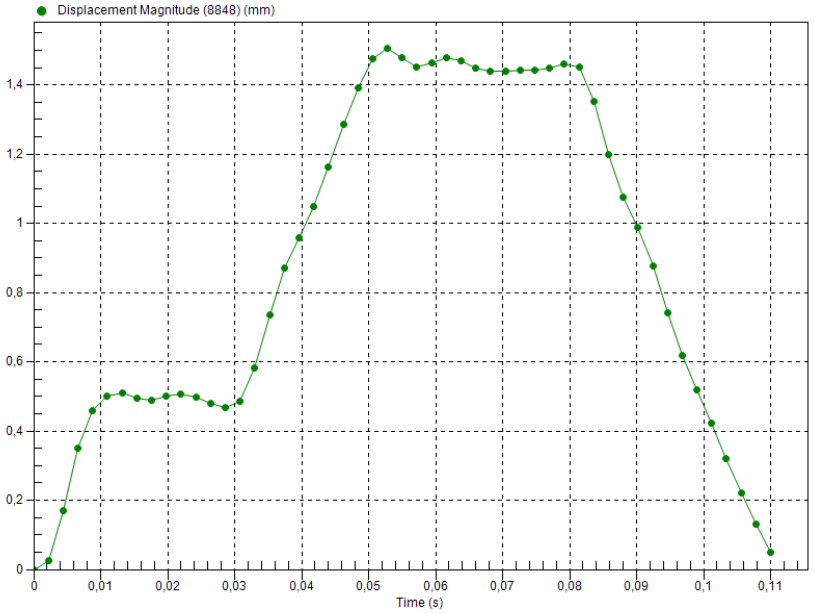

Figure 3.22 Graph of Total Displacement for Configuration 2 At the Right Side of Region 1

As can be observed from Figure 3.22, the maximum total displacement value for Configuration 2 when the camera holder locates at the right side of Region 1 is 1,5 mm.

The displacement graph in X direction for Configuration 2 when the camera holder locates at the right side of Region 1 is shown in Figure 3.23.

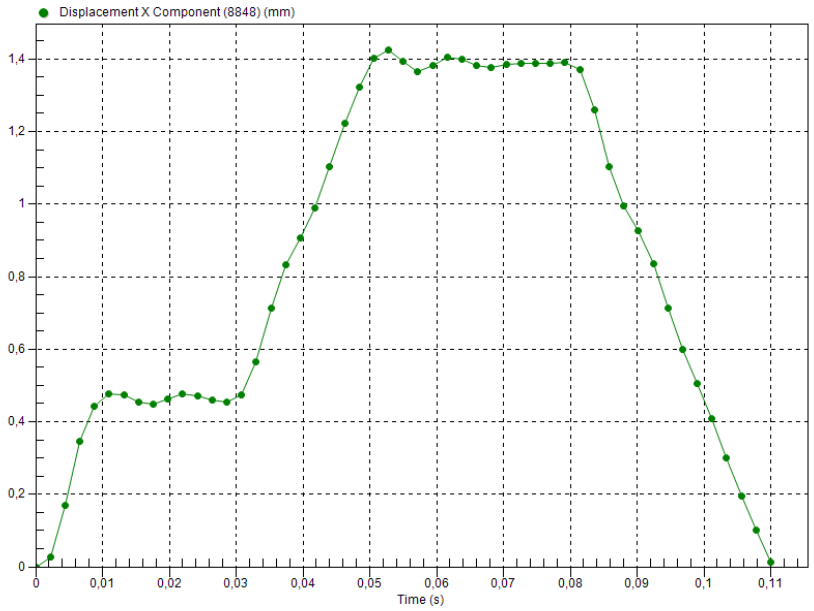

Figure 3.23 Graph of Displacement in X Direction for Configuration 2 At the Right Side of Region 1

As can be observed from Figure 3.23, the maximum displacement value in X direction for Configuration 2 when the camera holder locates at the right side of Region 2 is nearly 1,4 mm.

The displacement graph in Y direction for Configuration 2 when the camera holder locates at the right side of Region 1 is shown in Figure 3.24. As can be observed from Figure 3.24, the maximum displacement value in Y direction for Configuration 1 when the camera holder locates at the center of Region 2 is -0.49 mm.

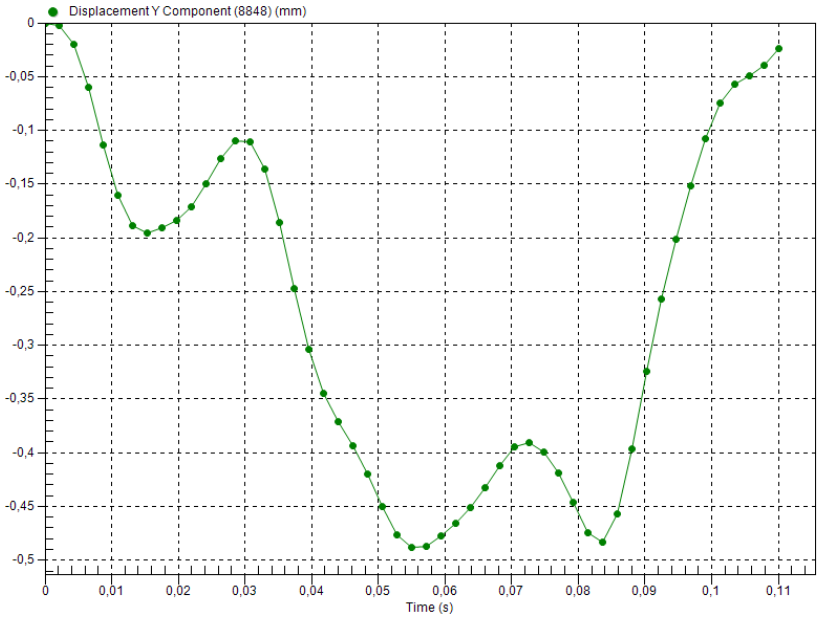

Figure 3.24 Graph of Displacement in Y Direction for Configuration 2 At the Right Side of Region 2

The displacement graph in Z direction for Configuration 2 when the camera holder locates at the right side of Region 1 is shown in Figure 3.25.

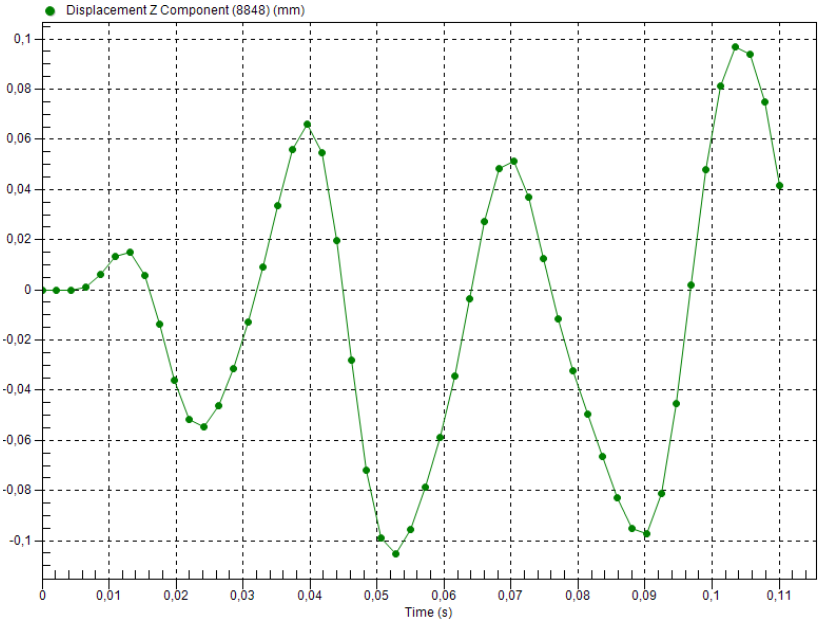

Figure 3.25 Graph of Displacement in Z Direction for Configuration 2 At the Right Side of Region 1

As can be observed from Figure 3.25, the maximum displacement value in Z direction for Configuration 2 when the camera holder locates at the right side of Region 2 is nearly -0.10 mm.

3.3.3 Displacement Graph for Configuration 3 at the Right Side of Region 3

The total displacement graph for Configuration 3 when the camera holder locates at the right side of Region 3 is shown in Figure 3.26.

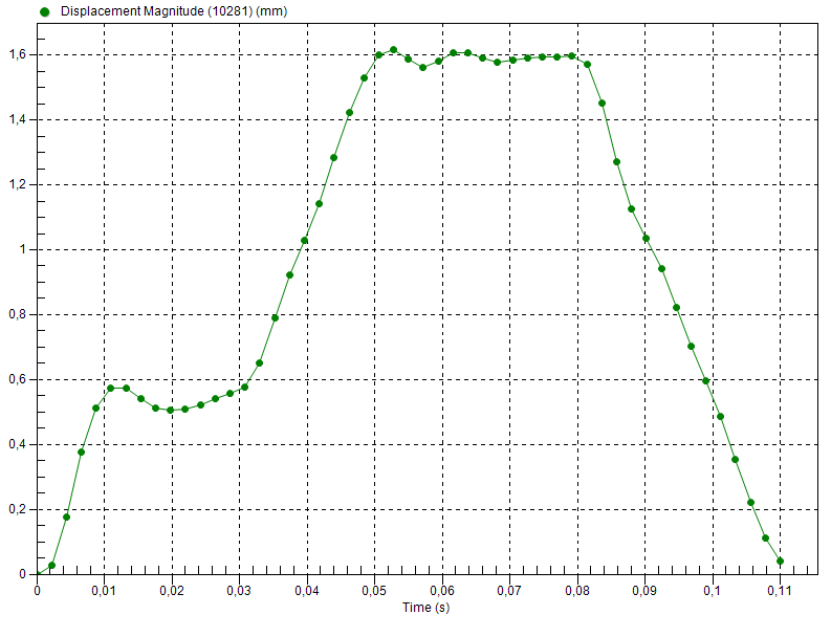

Figure 3.26 Graph of Total Displacement for Configuration 3 At the Right Side of Region 3

As can be observed from Figure 3.26, the maximum total displacement value for Configuration 3 when the camera holder locates at the right side of Region 3 is some bit above 1,6 mm.

The displacement graph in X direction for Configuration 3 when the camera holder locates at the right side of Region 3 is shown in Figure 3.27.

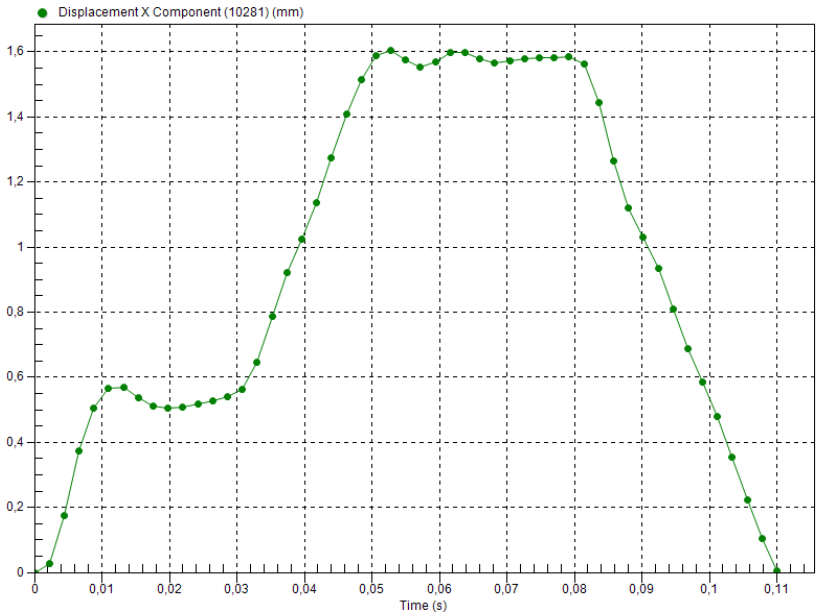

Figure 3.27 Graph of Displacement in X Direction for Configuration 3 At the Right Side of Region 3

As can be observed from Figure 3.27, the maximum displacement value in X direction for Configuration 3 when the camera holder locates at the right side of Region 3 is some bit below 1,6 mm.

The displacement graph in Y direction for Configuration 3 when the camera holder locates at the right side of Region 3 is shown in Figure 3.28. As can be observed from Figure 3.28, the maximum displacement value in Y direction for Configuration 3 when the camera holder locates at the center of Region 3 is some bit below -0.16 mm.

The displacement graph in Z direction for Configuration 3 when the camera holder locates at the right side of Region 3 is shown in Figure 3.29. As can be observed from Figure 3.29, the maximum displacement value in Z direction for Configuration 3 when the camera holder locates at the right side of Region 3 is some bit above -0.14 mm.

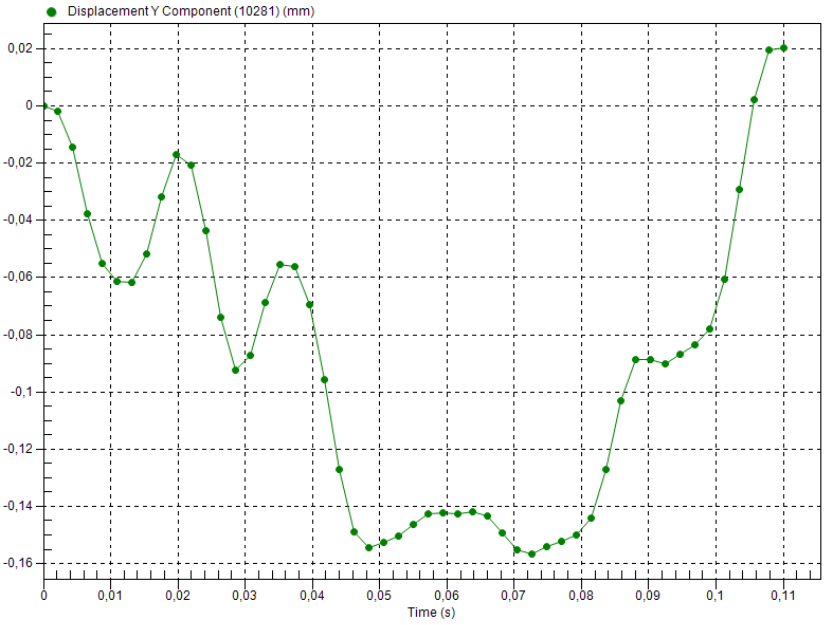

Figure 3.28 Graph of Displacement in Y Direction for Configuration 3 At the Right Side of Region 3

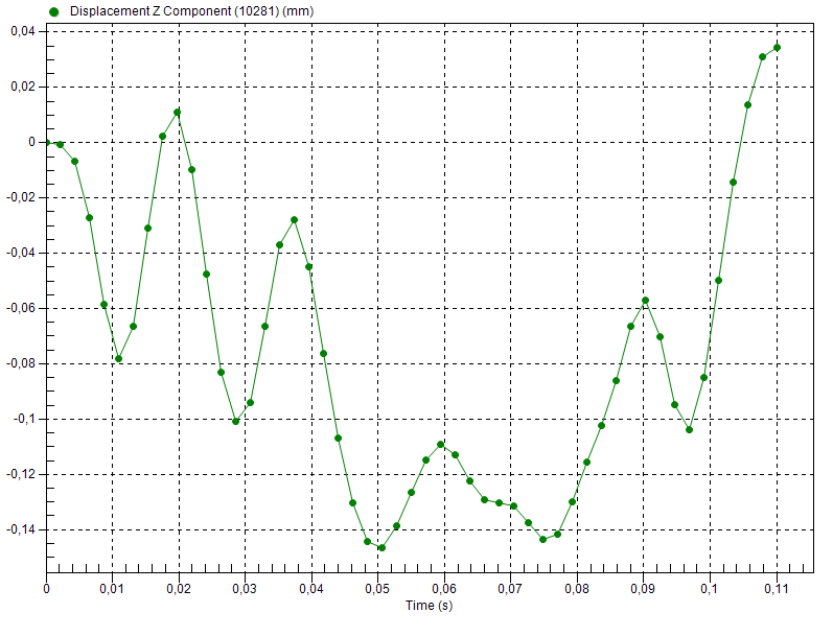

Figure 3.29 Graph of Displacement in Z Direction for Configuration 3 At the Right Side of Region 3

As a result of Figures 3.18 – 3.29, the maximum displacements occur between 50 milliseconds and 80 milliseconds where the enforced acceleration gets its maximum value of 90 g.

It is also seen that the most critical displacement occurs in X direction and the total displacement is highly affected by the displacement in X direction since the enforced acceleration is also applied in X direction.

In the analyses, the direct integration method is used because it is thought that the system will not face with vibration problems. Furthermore, the graphs shown on Figures 3.18 – 3.29 do not show any vibration characteristics due to their low magnitudes and non-repetitiveness during the test duration. Thus, it is reasable and verified to use direct integration method for this problem.

3.4 Stress Analysis for Camera Support Structure

The maximum Von Mises Stress values obtained on the whole camera support structure are tabulated in Table 3.6.

Table 3.6 Maximum Von Mises Stress Values in MPa

Regions	Region-1			Region-2			Region-3		
Sub Regions	Left	Center	Right	Left	Center	Right	Left	Center	Right
Configuration - 1	*	112	149	70	82	82	116	104	*
Configuration - 2	99	71	57	89	79	96	142	92	*
Configuration - 3	101	77	67	64	60	58	67	72	78

The stress values are quite below the yield strength of Aluminum 6063 T6 which is 215 MPa. Thus, there seems to be no problem in terms of structural strength.

3.5 Stress Distribution When the Maximum Stress Occurs

3.5.1 Stress Distribution for Configuration 1 at the Middle of Region 2

The Von Mises stress distribution in the camera support structure while the maximum stress occurs during the analysis is shown in Figure 3.30 for Configuration 1 when the camera holder is located in the middle of Region 2 and it is 82.83 MPa.

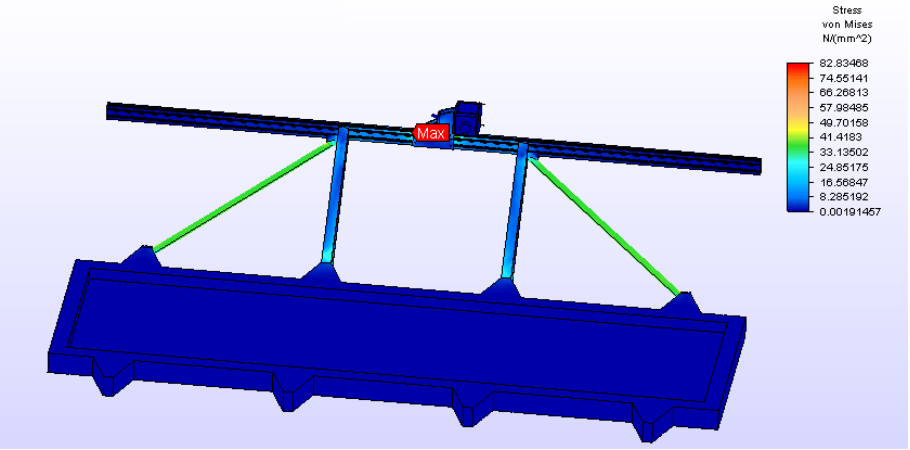

Figure 3.30 Graph of Stress Distribution for Configuration 1 At the Middle of Region 2

3.5.2 Stress Distribution for Configuration 2 at Right Side of Region 1

The Von Mises stress distribution in the camera support structure while the maximum stress occurs during the analysis is shown in Figure 3.31 for Configuration 1 when the camera holder is located in the middle of Region 2 and it is 57.47 MPa.

3.5.3 Stress Distribution for Configuration 3 at Right Side of Region 3

The Von Mises stress distribution in the camera support structure while the maximum stress occurs during the analysis is shown in Figure 3.32 for Configuration 1 when the camera holder is located in the middle of Region 2 and it is 78.97 MPa..

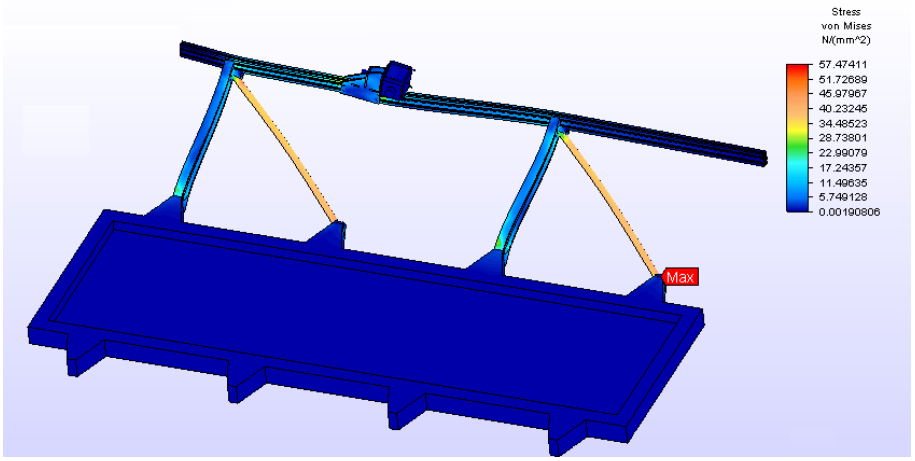

Figure 3.31 Graph of Stress Distribution for Configuration 2 At the Right Side of Region 2

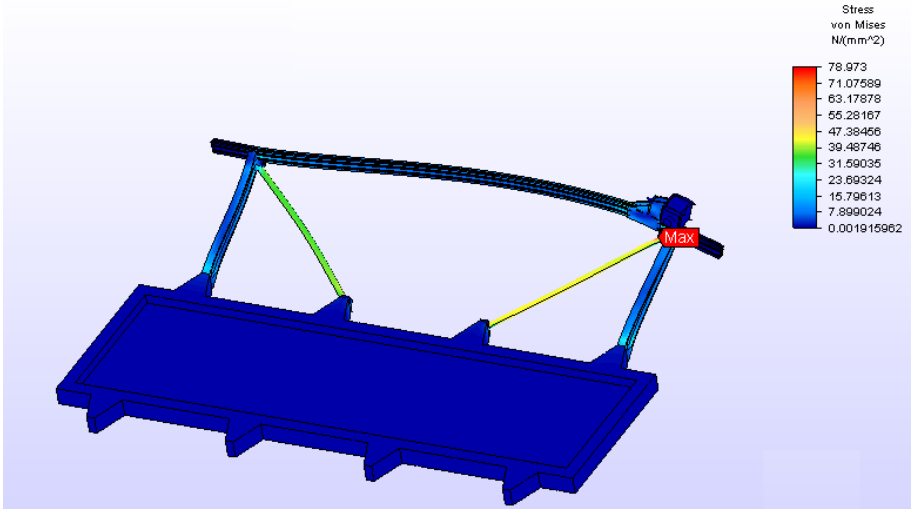

Figure 3.32 Graph of Total Displacement for Configuration 3 At the Right Side of Region 3

CHAPTER 4

ANALYSES FOR ALTERNATIVE CAMERA HOLDER PROFILE AND CAMERA HOLDER OF CAMERA SUPPORT STRUCTURE

As described in Chapter 2 and 3, three different configurations of camera support structure can be used. As tabulated in Table 3.5, Configuration 1 is recommended to be used in Region 2.

As seen in Figure 3.1, for Configuration 1, it seems that the length of the profile is very long and the side parts of the profile are unnecessary. In order to decrease the mass of the profile, it is more useful to use shorter profile. Thus, the system with short profile as shown on Figure 4.1 will be utilized for Configuration 1. If the analysis results of this design are better than the design with long profile, then for Configuration 1 this profile will be used.

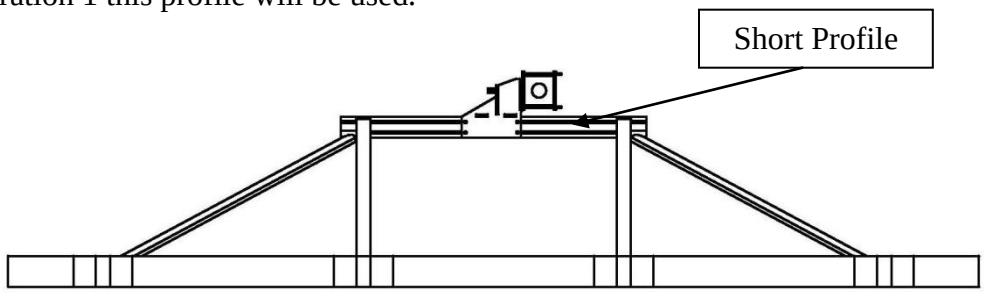

Figure 4.1 Configuration 1 with Short Camera Holder Profile

4.1 Analyses Results for Short Camera Holder Profile

The transient dynamic analysis is carried out for the camera support structure under Configuration 1 with short profile under the same enforced acceleration load as carried out with the long profile and the displacement results are tabulated in Table 4.1.

Table 4.1 Displacement Values with Long and Short Profiles at the Camera Lens Position

Displacement [mm]	Total	X – Direction	Y – Direction	Z – Direction
Short Profile	1.80	1.70	-0.45	-0.40
Long Profile	1.40	1.30	-0.29	-0.20

It seems to be surprising that the long profile has better results compared with the short profile. It is thought that since the short profile has less mass, its' results should be better than the long profile's results. It is useful to check the other displacement values on the camera holder. Thus, the displacement values on the camera holder base center as shown in Figure 4.2 will be tabulated and compared with the values acquired with the long profile.

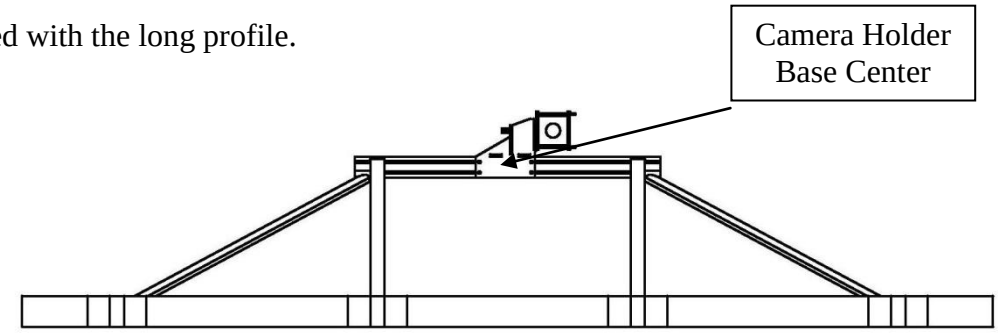

Figure 4.2 Camera Holder Base Center Position

The displacement values on the camera holder base center are tabulated in Table 4.2.

Table 4.2 Displacement Values with Long and Short Profiles at the Camera Holder Base Center

Displacement [mm]	Total	X – Direction	Y – Direction	Z – Direction
Short Profile	1.08	1.06	0.14	0.05
Long Profile	1.20	1.16	0.20	0.10

On the camera holder base center, the results are what were expected before the analyses. This shows that the displacement on the camera is more than the displacement on the camera holder base. This difference is the result of a rotation on

the camera lens position because of the design of the camera holder. Having more mass on the profile will result in less rotation on the camera lens position and hence less displacement. The camera lens position is more critical than the camera holder base and the alternative design has not brought any advantages over the long profile in terms of displacement. Therefore, it is reasonable to use long profile in this camera support structure.

The exaggerated displacement model shapes for both designs are shown on Figure 4.3 and Figure 4.4.

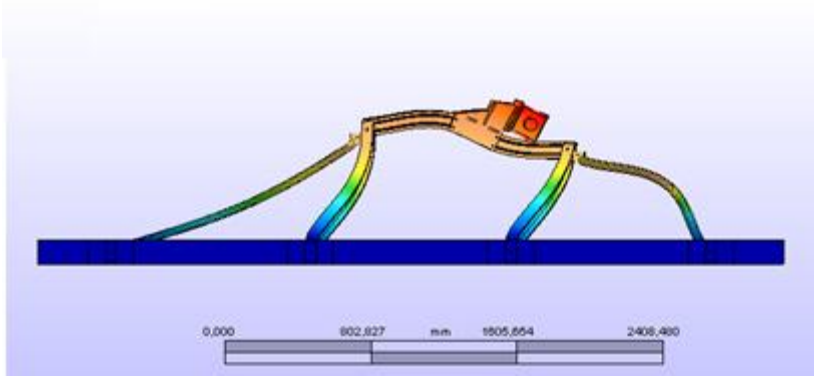

Figure 4.3 Exaggerated Displaced Model Shape for Short Profile

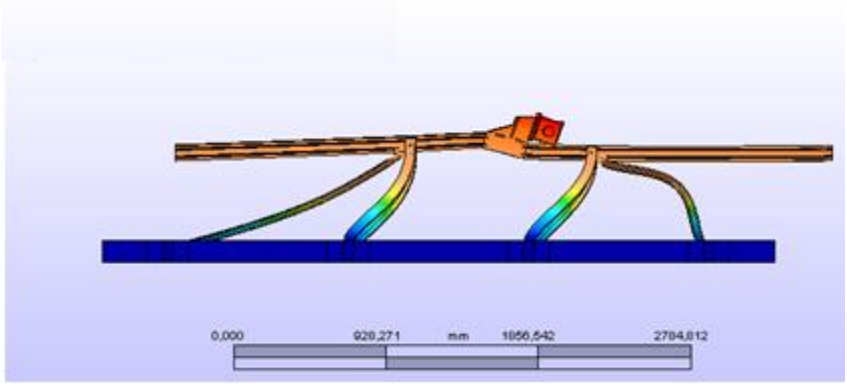

Figure 4.4 Exaggerated Displaced Model Shape for Long Profile

4.2 Analyses for Alternative Camera Holder Design

As discussed in the previous section, short profile does not show better results as expected and this may be from the design of the camera holder. If the camera holder have such a design that the centers of gravity of the camera and the camera holder system coincides, the rotation effect on the camera will be smaller. To satisfy this design criterion, an alternative camera holder design may be suggested. The easiest way to satisfy this design criterion is to hold the camera from the both sides. In order not to have very heavy structure, sides of the camera holder are modified as shown in Figure 4.5.

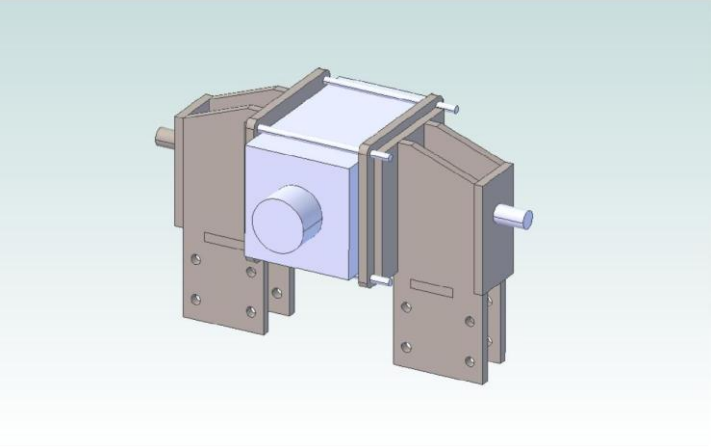

Figure 4.5 New Camera Holder Design

The original camera holder weighs 4600 grams whereas the alternative camera holder weighs 5550 grams. All the dimensional details of the original and alternative camera holder are shown in Appendix C.

The alternative camera holder is analyzed with both long and short camera holder profiles. All the analyses are carried out for Configuration 1 with camera holder positioned in the center of Region 2.

The displacement results for short camera holder profile and long camera holder profile with the alternative camera holder design is tabulated in Table 4.3, whereas

the displacement values with the original camera holder design are tabulated in Table 4.4.

Table 4.3 Displacement Values with the Alternative Camera Holder

Displacement Values [mm]	Total	X – Direction	Y – Direction	Z – Direction
Short Profile	1.40	1.39	-0.04	-0.01
Long Profile	1.36	1.30	-0.05	-0.11

Table 4.4 Displacement Values with the Original Camera Holder

Displacement Values [mm]	Total	X – Direction	Y – Direction	Z – Direction
Short Profile	1.80	1.70	-0.45	-0.40
Long Profile	1.40	1.30	-0.29	-0.20

As observed from the above values, with the new camera holder design, the displacement values are improved for short profile at a high percentage and there is a slight improvement for the long profile. With the new camera holder design, the short profile displacement values are very near to the long profile displacement values although the weight of the alternative camera holder is larger than the original camera holder.

Although the values are improved for short profile, under these conditions it is not reasonable to use short profile with the alternative camera holder design. The displacement values achieved with the short profile and alternative camera holder design do not worth to use them for the tests. The values are not better than the values achieved with the long profile and the original camera holder.

CHAPTER 5

TESTS ON SLED CRASH TEST SYSTEM

All the finite element analyses are carried out with the maximum acceleration of 90 g which is the maximum applicable acceleration achieved in the crash test system at METU-BILTIR Crash Test Facility. According to the analyses results, the camera support structure can withstand the load experienced under 90 g acceleration. Therefore, it can be said that the camera support structure system can also withstand acceleration loads lower than 90 g. Most of the tests in METU-BILTIR Crash test facility are carried out with nearly 40 g maximum accelerations, thus the tests are performed under this maximum acceleration in order not to force the limits of the sled crash test system. Due to the economic aspects of the tests, the test is performed only for Configuration I and the camera holder is positioned in the middle of region 2. In order to compare the test results with the analyses results, finite element analysis is carried out for Configuration 1 having the camera holder being positioned in the middle of Region 2 under 40 g maximum acceleration.

5.1 Tests with the Dummy Camera

Since the high-g high speed cameras used in crash tests are very expensive, in order not to harm the camera in the first test, dummy camera was designed and used. After the successful run of the test with the dummy camera, real high-g high speed imaging camera can be used and the test can be recorded.

3.5.4 Dummy Camera

Dummy camera is similar with the original high-g high speed imaging camera in physical properties, such as weight, dimension and center of gravity. The camera is constructed with 4 mm thickness aluminum sheets and in order to have similar center

of gravity with the original camera, rectangular aluminum block is welded inside the closed box. The dummy camera is shown in Figure 5.1.

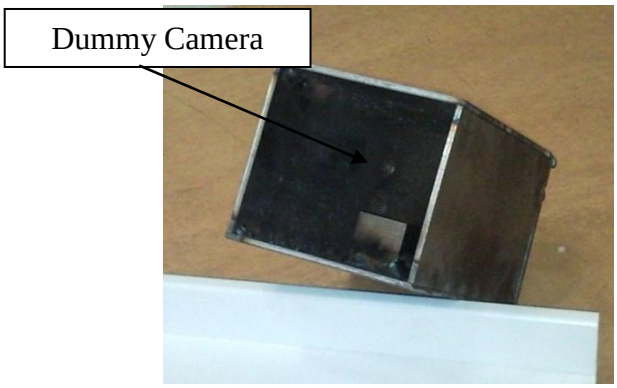

Figure 5.1 Dummy Camera

3.5.5 Test System with the Dummy Camera

The test system was constructed with the dummy camera as shown on Figure 5.2.

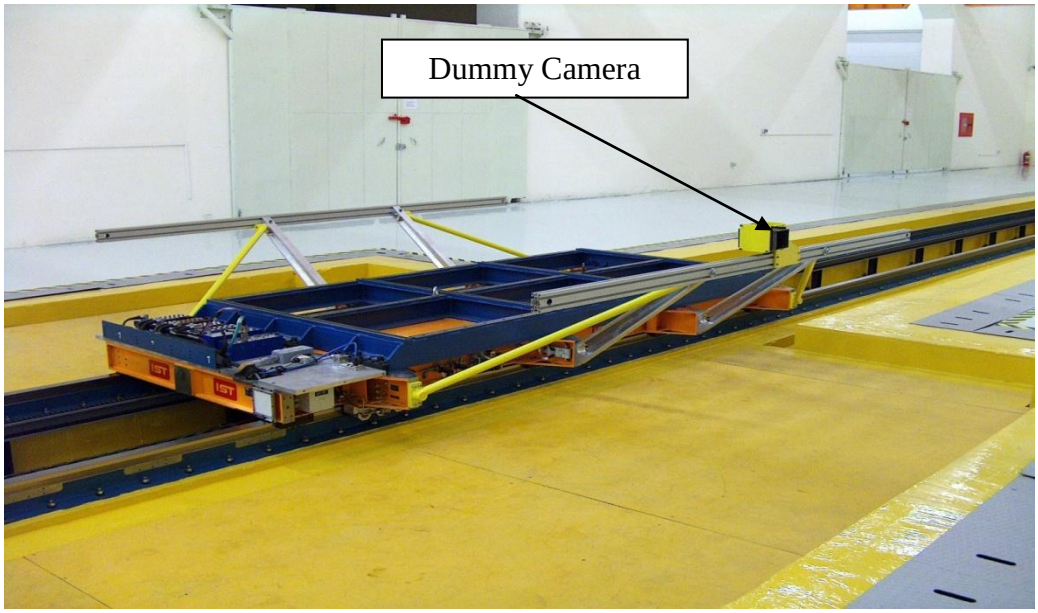

Figure 5.2 Crash Test System with the Dummy Camera

3.5.6 Off-Board Cameras Used During the Test

Two off-board cameras were used during the test.

The first one shown in Figure 5.3 was on the ground and was focused directly to the dummy camera in order to inspect its behaviour during test.

Figure 5.3 Off-Board Camera on the Ground

The second one shown in Figure 5.4 was infront of the catapult and was recording from the side of the profile in order to inspect the fluctuation behaviour of the camera during the test. The fluctuations can be easily seen from this camera.

Figure 5.4 Off-Board Camera in front of the Catapult

3.5.7 Pulse Generation for the Test

According to the total mass on the sled crash test system, to obtain the target acceleration curve, pulse should be generated prior to the test. Pulse generation operations were repeated four times to obtain the target curve before the test. As a result of these repeated operations, final pulse generated is shown on Figure 5.5.

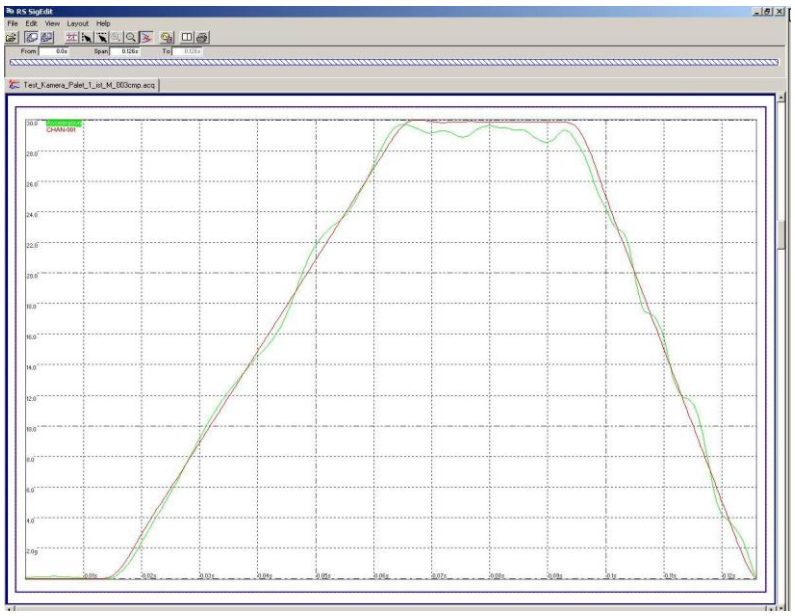

Figure 5.5 Final Pulse Generated Before the Test

3.5.8 Test Results

According to the test results, there seem to be no problems in structural means. Thus, it is reasonable to continue with the real high-g high speed imaging camera. By this way, it can be observed whether the fluctuation of the high speed imaging camera on profile is enough for good record of the test or not.

5.2 Test with High-g High Speed Imaging Camera

There occurred no problems in the test with the dummy camera. This implies that there will occur no problems during the usage of the high-g high speed imaging camera in the test. The crash test system constructed with the high-g high speed imaging camera is shown on Figure 5.6.

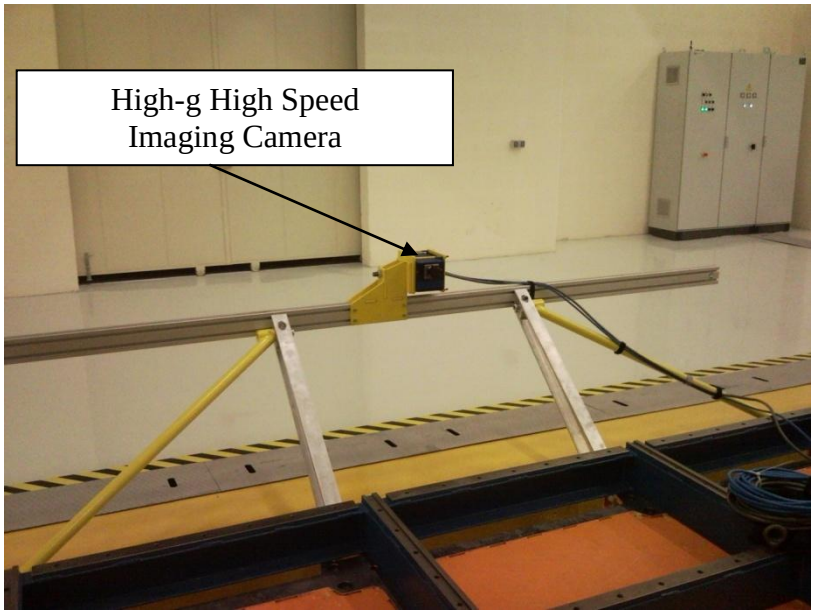

Figure 5.6 The Crash Test System with High-g High Speed Imaging Camera

In this test, we have one on-board and one off-board camera. The off-board camera preserved its position in front of the catapult as in the test with the dummy camera and recorded the event from the side of the profile. From the record of the onboard camera, the position of the camera holder can be easily observed. Before the run of the test, all the cables are fixed tightly in order to keep them fixed during the high-g test.

Since the pulse has been generated for the test with dummy camera and the physical properties of the dummy camera and the high speed high-g imaging camera are same, the test was directly performed.

CHAPTER 6

CONCLUSIONS AND DISCUSSIONS

6.1 General Conclusion

Three different configurations of camera support structure are used at METU-BİLTİR Crash Test Facility. The camera holder may be located on different positions on the camera holder profile in these configurations. As a result of finite element analyses presented for three different configurations of the camera support structure with different camera holder position cases, the followings are concluded.

1. The displacement results showed that,
   a. Configuration 2 should be used with the camera holder located at the right side of the Region 1.
   b. Configuration 1 should be used with the camera holder located at the middle of the Region 2.
   c. Configuration 3, should be used with the camera holder located at the right side of the Region 3.

2. Within all of the configuration and camera holder position cases, the minimum displacement is obtained with Configuration 1 when the camera holder is located in the middle of Region 2.

3. The displacement graph of the camera lens center shows that there is no vibration on the camera support structure.

4. An alternative analysis is carried out for Configuration 1 in Region 2 by removing the sides of the camera holder profile. However, the analyses results show that higher deflections occurred for the camera lens center. This

leads to the design of an alternative camera holder. The analyses results obtained with the short camera holder profile and the new camera holder do not show any improvement in the displacement values.

5. According to the finite element analyses results, the camera support structure is found to be satisfactory during the crash tests. Two sled crash tests have been carried out at METU-BİLTİR Crash Test Facility by using a dummy camera and a high-g high speed imaging camera. The dummy camera is designed in such a way that it has similar weight, volume and center of mass with the original camera. After the verification with the dummy camera, the original high-g high speed imaging camera is used in the other test. The tests are recorded with high-g high speed cameras and it has been observed that there is no vibration that prevents imaging and the strength of the system is satisfactory.

6. The computer analyses and the tests performed at the METU-BİLTİR Center Vehicle Safety Unit showed that, the camera support structure can be safely used for the suggested configuration and camera holder positions.

6.2 Future Works

The test at METU-BİLTİR Crash Test Facility has been carried out only for one test pulse with a value of 30 g maximum acceleration and for one configuration and one camera holder position case. In future works, all the possibilities of camera holder support structure configurations and related camera holder position cases may be also tested for different test pulse curves.

The tests are recorded by high-g high speed imaging cameras, but there is no ability to further investigate the recorded videos. In order to get detailed information for the behavior of the camera during the test, there are two possibilities that may be carried in future works. One is to use displacement transducers during the test; the other one is to use Visualization Analysis software after the test.

By using displacement transducers in the test system, it is possible to record the displacement of the camera lens during the test. Displacement transducers are placed at the camera lens center position and they record the displacement of the camera lens center position during the test in three axes of the system as X, Y and Z.

Furthermore, the behavior of the camera lens center position during the test may also be investigated by using Visualization Analysis software. Bu using this type of software, the displacement behavior of the camera lens center position may be investigated from the recorded videos.

As a result of the detailed information for the displacement of the camera lens center position, the displacement outputs from the above methods may be compared with the displacement results obtained in finite element analyses.

In this study, the high-g high speed camera is used on the camera support structure outside the test sample. In some cases, it may be needed to use onboard high-g high speed cameras within the test sample in order to get detailed information from the inside of the structure. For these applications, in future works new onboard camera holders may be designed and the designs may be verified with finite element analyses.

REFERENCES

[1] Holmes, Gillian. "Crash Test Dummy." How Products Are Made. Gale Research Inc. 2000.

[2] Crash Test, website: “http://en.wikipedia.org/wiki/Crash_test”, last accessed: 17 March 2009

[3] Developing a Sled Test from Crash Test Data, Paper, Brian Smyth and James Smith Exponent Inc., April 2007

[4] ECE Regulations, website: “http://www.crashnetwork.com”, last accessed: 20 May, 2009

[5] Euro NCAP, website: http://en.wikipedia.org/wiki/Euro_NCAP, last accessed: 10 June 2009

[6] Ulaş Göçmen, “Experimental Analysis in Crash Test”, Ms Thesis, Middle East Technical University, Ankara, September 2009

[7] Alan M. Nahum, John Melvin, “Accidental Injury: Biomechanics and Prevention”, Springer, New York, 2002

[8] Kirsten Larsen, “DTS Data Point”, DTS Publication, 2008

[9] Lighting for High Speed Imaging, website: “http://www.visinst.com”, last accessed: 10 March 2009

[10] System Guide, website: http://www.crash-network.com”, last accessed: 04 April 2009

[11] Transient Dynamic Analysis, “Algor User Guide”, Algor Inc., Pittsburgh, 2008

[12] Zienkiewicz OC, Taylor RL, “The Finite Element Method”, McGraw-Hill, New York, 2000

[13] Swapan Kumar Nandi, Sudeep Bosu, “Effect of Mass Matrix Formulation Schemes on Dynamics of Structures”, Paper, 2007

[14] Explicit and Implicit methods, “http://en.wikipedia.org/wiki/”, last accessed: 15 April 2009

[15] Brian Clark, “The Behavior of Rollover Protective Structures subjected to Static and Dynamic Loading Conditions”, PhD. Thesis Study, November 2005

[16] B.Tasi´c, R.M.M.Mattheij, “An Explicit Method for Solving Flows of ODE”, Eindhoven University of Technology, Ms Thesis, March 2008

[17] Torque Values for Bolts and Screws, “http://www.ascivata.com”, last accessed: 15 April 2009

[18] Typical Acceleration Graph used in Crash Tests

[19] Instron Structural Testing Systems, website: “www.instron.com/ist/”, last accessed: 08 July 2009.

[20] Weinberger Vision, website: “www.weinbergervision.com”, last accessed: 19 October 2009.

[21] KT Automotive, website: “www.kt-automotive.com”, last accessed: 08 July 2009.

APPENDIX A

TECHNICAL INFORMATION OF CAMERA SUPPORT STRUCTURE COMPONENTS AT METU-BİLTİR CENTER VEHICLE SAFETY UNIT

A.1 Technical Specifications of Camera Holder Support Arms

The camera holder support arm shown in Figure A.1 is composed from four different components. All of these components are machined from Aluminum 6063-T6 separately and then welded together to form the camera holder arm. All the dimensions are given in mm.

The first component is a hollow cylindrical part and the technical drawing is shown in Figure A.2.

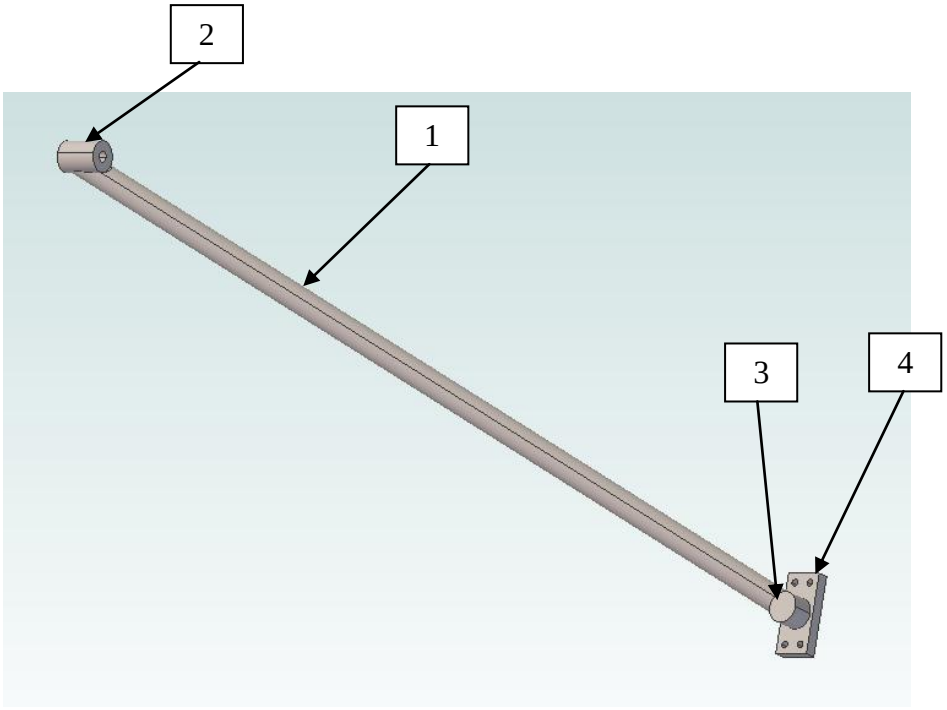

Figure A.1 Camera Holder Support Arm

The weight of the camera holder support arm is 7684 grams.

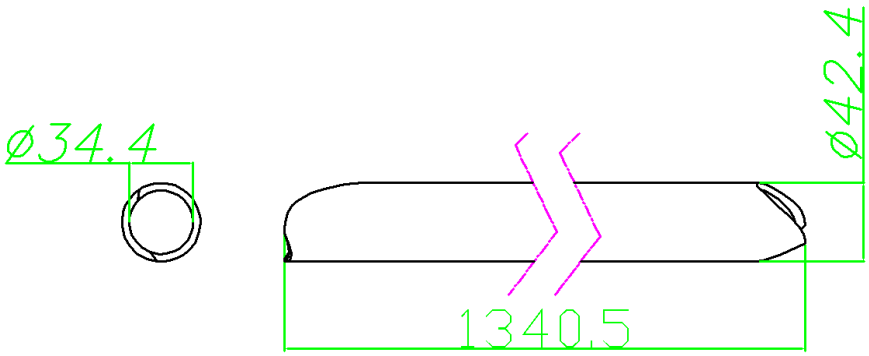

Figure A.2 Technical Drawing of the First Component

The second component is also a hollow cylindrical part and the technical drawing is shown in Figure A.3.

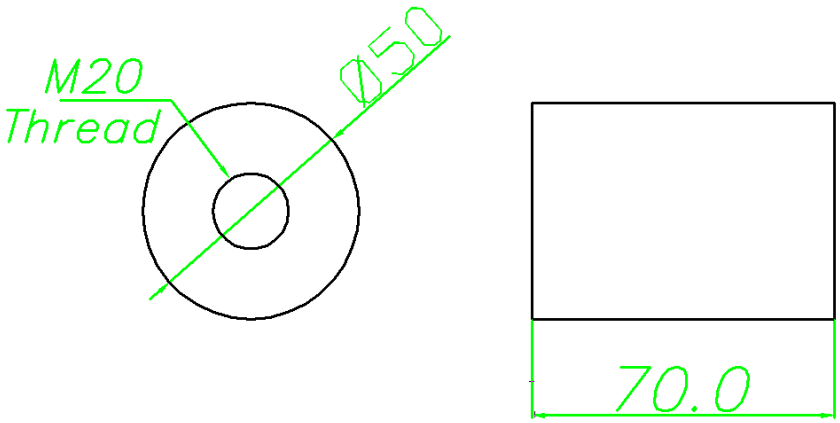

Figure A.3 Technical Drawing of the Second Component

The third component is similar to the second component except the M20 thread in the center of the part. The technical drawing is shown in Figure A.4.

Finally, the forth component is a rectangular component and there are screw holes on it in order to fix the camera holder arm to the sled. The technical drawing is shown in Figure A.5.

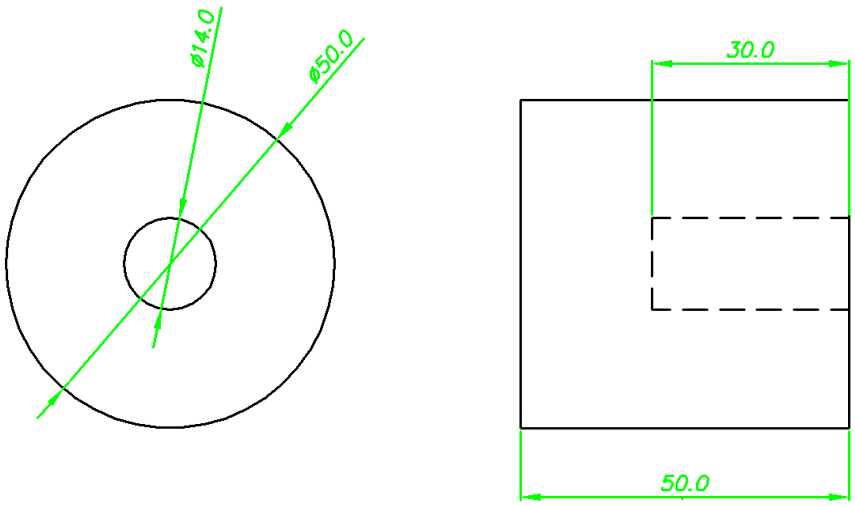

Figure A.4 Technical Drawing of the Third Component

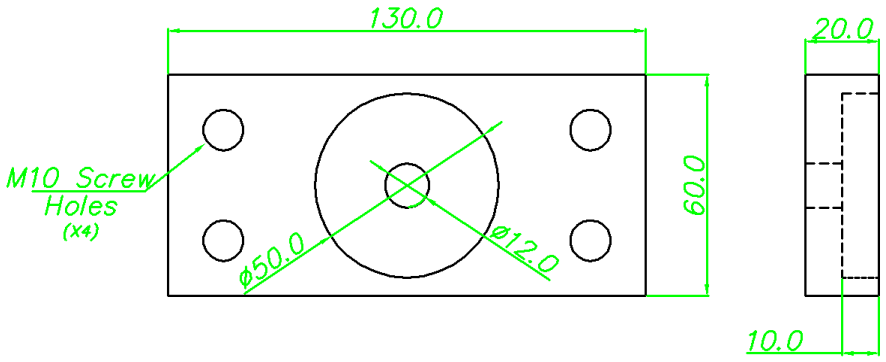

Figure A.5 Technical Drawing of the Forth Component

A.2 Technical Specifications of Camera Holder Arms

The camera holder arm shown in Figure A.6 is machined from Aluminum 6063-T6. There are some screw holes in order to secure it to the sled and also to secure camera holder support arm and camera holder profile to it. The technical drawing is shown in Figure A.7. All the dimensions are given in mm.

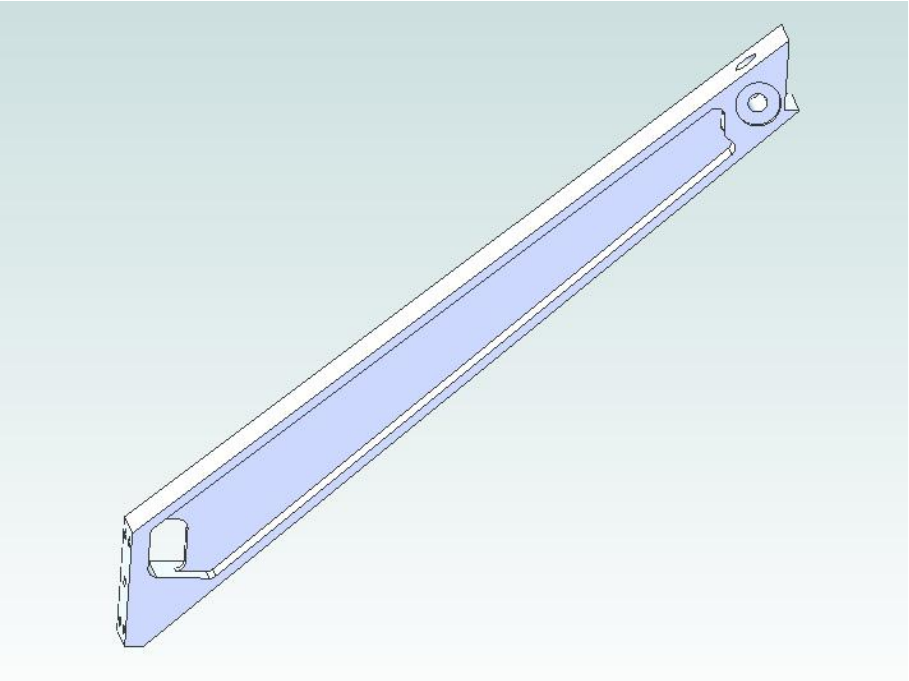

Figure A.6 Camera Holder Arm

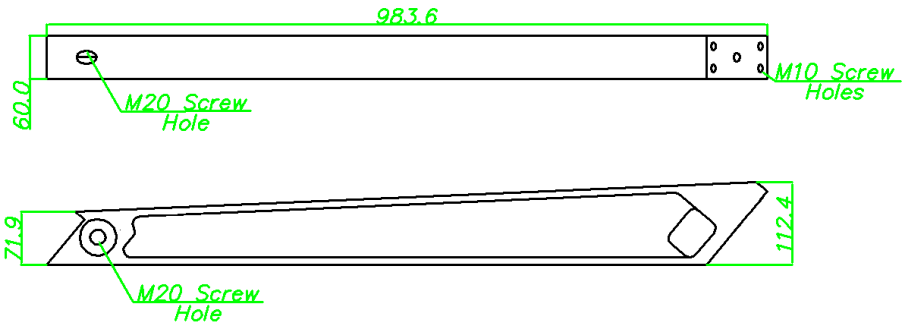

Figure A.7 Technical Drawing of Camera Holder Arm

The weight of the camera holder arm is 5820 grams.

A.3 Technical Specifications of Camera Holder Profile

The camera profile shown in Figure A.6 is a standard structural member. The camera holder can slide on it easily. After the desired position for the camera holder is achieved, it is fixed to the camera holder profile together with the camera. All the dimensions in Figure A.8 are given in mm.

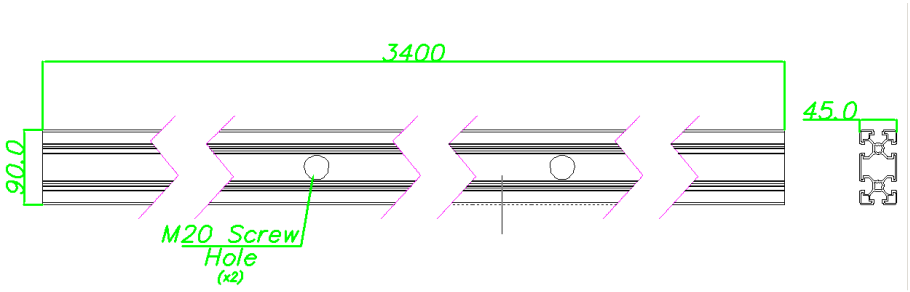

Figure A.8 Technical Drawing of Camera Holder Profile

The weight of the camera holder profile is 10999 grams.

A.4 Technical Specifications of Camera Holder

The camera holder shown in Figure A.1 is composed from four different components. All of these components are machined from 10 mm sheet Aluminum 6063-T6 separately and secured together to form the camera holder. All the dimensions are given in mm.

The first component forms the one side of the camera holder base and the third component is secured to it. The technical drawing is shown in Figure A.2.

The second component is similar to the first component and it forms the other side of the camera holder base. The technical details are shown in Figure A.11.

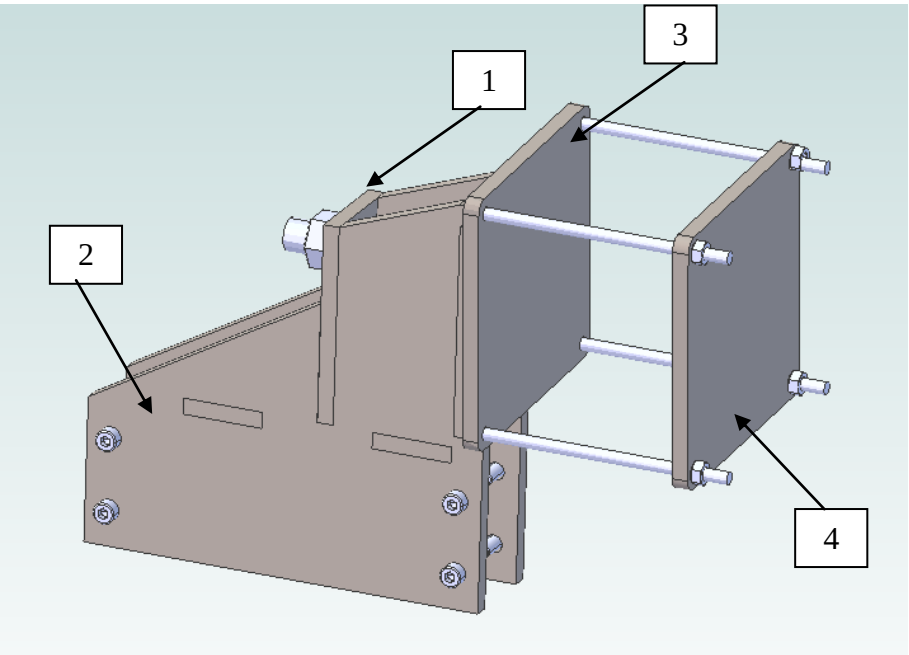

Figure A.9 Camera Holder

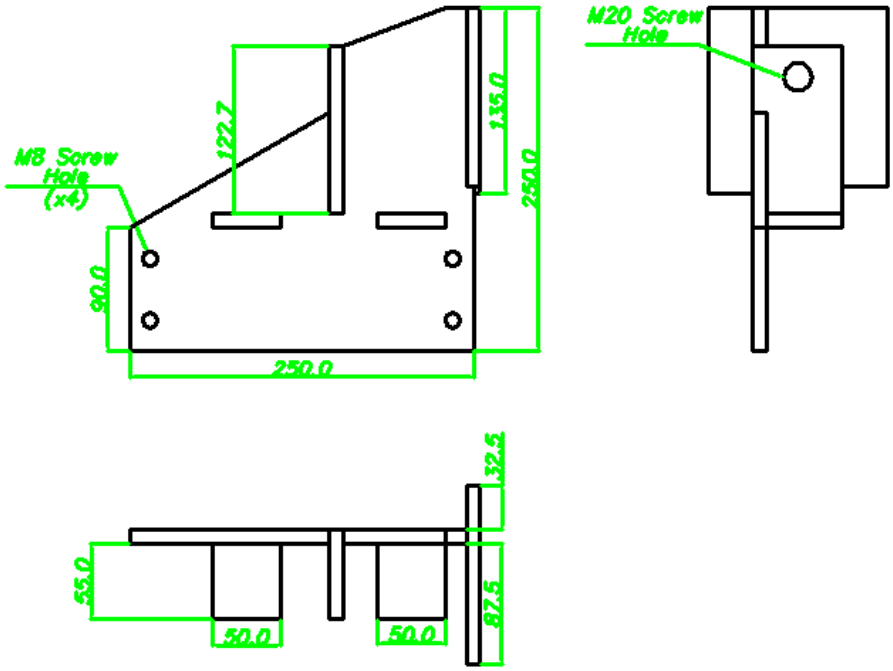

Figure A.10 Technical Drawing of the First Component of Camera Holder

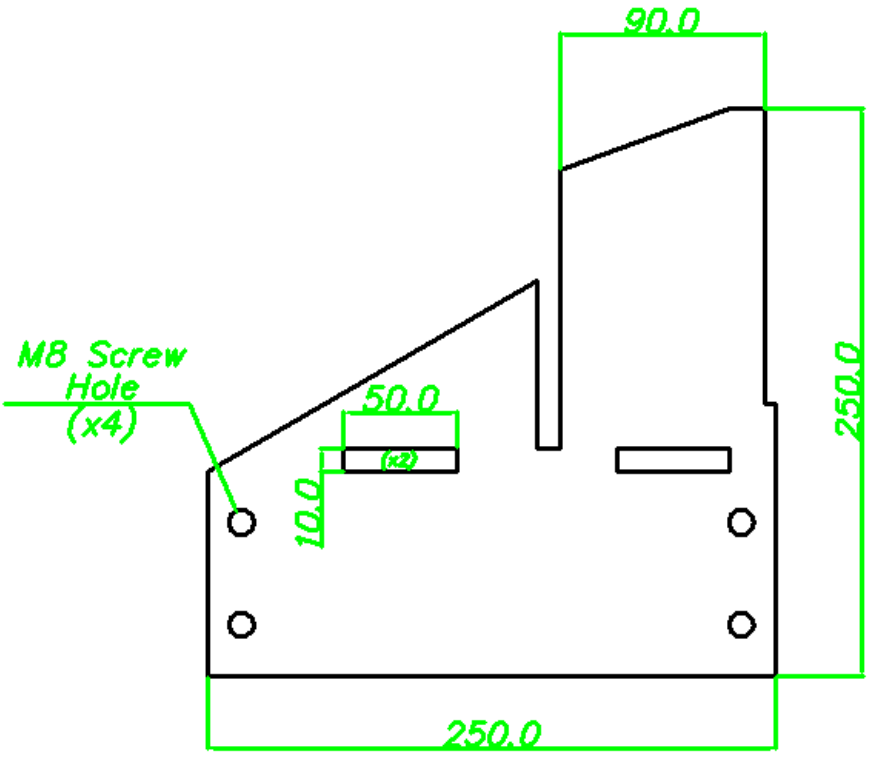

Figure A.11 Technical Drawing of the Second Component of Camera Holder

The third component is secured to the first component and it forms one side of the camera holder. The technical details are shown in Figure A.12.

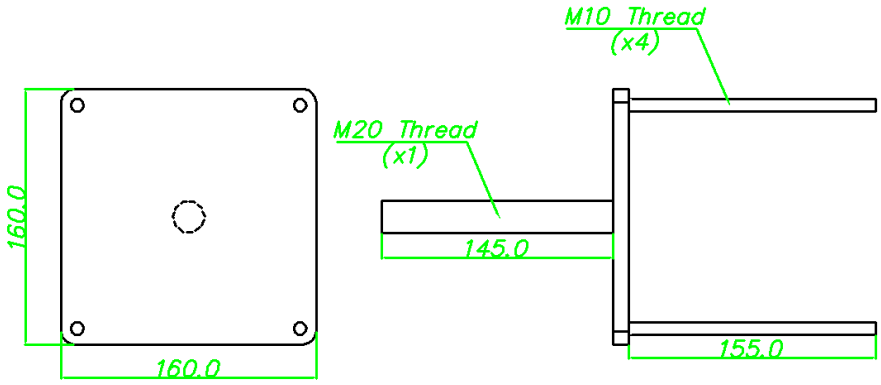

Figure A.12 Technical Drawing of the Second Component of Camera Holder

The forth component is secured to the third component and it forms the other side of the camera holder. The camera is clamped between the third and forth component. The technical details are shown in Figure A.13.

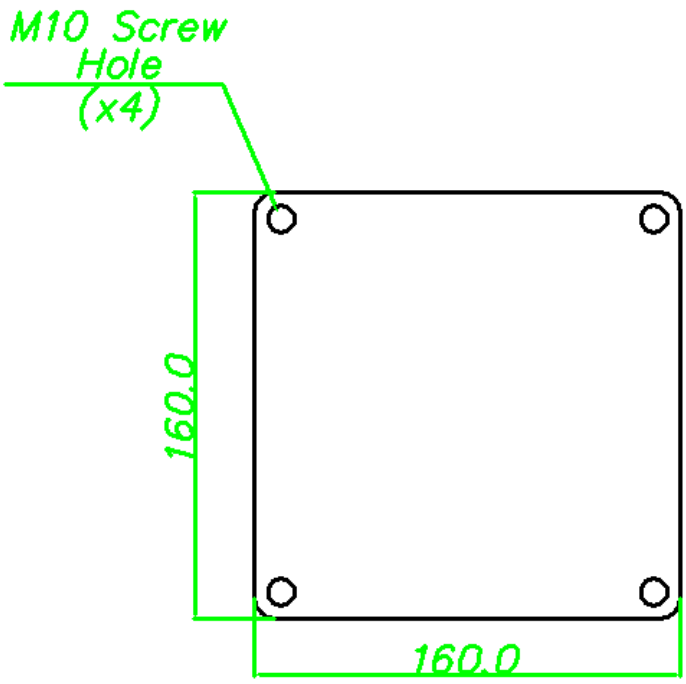

Figure A.13 Technical Drawing of the Second Component of Camera Holder

The total weight of the camera holder is 4605 grams.

APPENDIX B

TECHNICAL INFORMATION OF SLED CRASH TEST SYSTEM, HIGH SPEED CAMERA AND DATA ACQUISITION SYSTEM AT METU-BİLTİR CENTER VEHICLE SAFETY UNIT

B.1 Technical Specifications of IST Sled Crash Test System [19]

Technical Specifications:

Catapult Actuator Unit:

- 2500 kN nominal force
- 1700mm working stroke
- 140.000 l/dk 4-stage Servovalf
- 2500 kg max. payload

Sled and Rail System:

- 32m. long precise rails
- 1800 x 4100 mm sled dimensions

Hydraulic Power Pack:

- 250 l/min flow capacity
- 290 bar pressure

Performance:

- 90 g max. acceleration
- 90 km/hr max. velocity

B.2 Technical Specifications of Weinberger Vision Visario G2 High Speed Camera [20]

Based upon the world-wide proven Weinberger Vision Visario industry standard, the compact and lightweight systems of the second generation (G2) unite to provide a rare wealth of performance features. It is designed for high end operation in the fields of automotive, military and research and development.

Technical specifications of the Visario G2 camera:

- High Speed APS CMOS Sensor
- 1536 x 1024 resolution at 1.000 fps
- Maximum 10.000 fps at reduced resolutions
- 10µs global electronic shutter
- Fast Gigabit Ethernet interface
- Monochrome 10 bit, color depth up to 30 bit
- 25 Watt power consumption
- Lens Mounts: C, F, Box and Custom
- Weight: 7.8 lbs.
- Size: 113 x 120 x 200 mm
- Rated at 100g's in all three axes

- Embedded LINUX operating system

B.3 Technical Specifications of Kayser Threde Minidau Advanced Data Acquisition System [21]

The Minidau Advanced used during test has 32 analog channnels of which 16 of them can also be used as digital channels. Each analog channel comprises a programmable input amplifier, bridge excitation, 16 bit A/D converter for simultaneous sampling. The amplifier gain precision is better than 0.2% and the input impedance above 10 MOhm. The gain values can be programmed in steps from 1 to 10000. An internal reference voltage is used for precise control of the amplifier setting. Neither potentiometers nor trimmers nor mechanical switches are used inside the device. All adjustments are implemented by software, automatically or by command.

The bridge excitation voltage is programmable separately for each channel. All 8 channels of an amplifier board can be used for the classical voltage excitation modes. Four out of these channels can deliver extended excitation modes. This includes a high voltage mode up to 20 V and a constant current excitation mode. Bridge completion for half bridges can be switched internally .

Shunt measurement and check is implemented as a full 4 quadrant circuit with internal emulation of customer specific shunt resistor values. External shunt resistors are supported as well.

The signal bandwith of the amplifier has been extended to 42,5 kHz. With conventional designs this would require sampling rates above 200 kHz. Due to the state of the art oversampling A/D converter design including adaptive filtering this bandwidth of the amplifier can be efficiently used sampling at 100 kHz. This feature allows the measurement of acoustic events e.g. due to airbag inflation during the crash. test.

The Minidau Advanced amplifier introduces an overload detection. It is implemented between the amplifier part and the filter part removing high frequency disturbing

signals. Overload conditions are sampled and stored together with the actual measurement data to allow in deep study of this phenomenon.

In contrast to former designs, the low-pass filter is a pure anti-aliasing filter with an adaptive cutoff frequency that fits to the currently selected sampling frequency. All necessary additional filtering, e.g. according to SAE filter classes, is done during post processing.

Sampling and Storage of measurement data has been implemented similar to the proven design of the conventional Minidau, using volatile sram memory during pretrigger and non volatile Nand flash memory for data storage. Batteries are not needed to retain the data. The Minidau Advanced can store data for a 50s cycle even at the full sampling rate of 100kHz which allows the user to start recording data before the vehicle or sled is actually started. This ensures that the measuring system functions correctly and prevents data loss, even in case of possible malfunctions of the trigger signal. This is the main error cause, apart from user errors. The trigger point is registered and recorded. Once a valid trigger point is stored in the Minidau Advanced data memory, the user can select only the actual measured data for transfer to a PC, it is not necessary to read out the complete data memory.